Tellus SERIES A DYNAMIC METEOROLOGY AND OCEANOGRAPHY
PUBLISHED BY THE INTERNATIONAL METEOROLOGICAL INSTITUTE IN STOCKHOLM

Quantitative precipitation estimation based on high-resolution numerical weather prediction and data assimilation with WRF – a performance test

By HANS-STEFAN BAUER[1]*, THOMAS SCHWITALLA[1], VOLKER WULFMEYER[1], ATOOSSA BAKHSHAII[1], UWE EHRET[2], MALTE NEUPER[2] and OLIVIER CAUMONT[3], [1]*Institute of Physics and Meteorology, University of Hohenheim, Garbenstrasse 30, DE-70599 Stuttgart, Germany*; [2]*Institute of Water and River Basin Management, Section Hydrology, Karlsruhe Institute of Technology, Otto-Amman-Platz 1, DE-76131 Karlsruhe, Germany*; [3]*CNRM-GAME (Météo-France and CNRS), 42, Av. G. Coriolis, FR-31057 Toulouse Cedex 1, France*

(Manuscript received 27 May 2014; in final form 10 March 2015)

ABSTRACT

Quantitative precipitation estimation and forecasting (QPE and QPF) are among the most challenging tasks in atmospheric sciences. In this work, QPE based on numerical modelling and data assimilation is investigated. Key components are the Weather Research and Forecasting (WRF) model in combination with its 3D variational assimilation scheme, applied on the convection-permitting scale with sophisticated model physics over central Europe. The system is operated in a 1-hour rapid update cycle and processes a large set of in situ observations, data from French radar systems, the European GPS network and satellite sensors. Additionally, a free forecast driven by the ECMWF operational analysis is included as a reference run representing current operational precipitation forecasting. The verification is done both qualitatively and quantitatively by comparisons of reflectivity, accumulated precipitation fields and derived verification scores for a complex synoptic situation that developed on 26 and 27 September 2012. The investigation shows that even the downscaling from ECMWF represents the synoptic situation reasonably well. However, significant improvements are seen in the results of the WRF QPE setup, especially when the French radar data are assimilated. The frontal structure is more defined and the timing of the frontal movement is improved compared with observations. Even mesoscale band-like precipitation structures on the rear side of the cold front are reproduced, as seen by radar. The improvement in performance is also confirmed by a quantitative comparison of the 24-hourly accumulated precipitation over Germany. The mean correlation of the model simulations with observations improved from 0.2 in the downscaling experiment and 0.29 in the assimilation experiment without radar data to 0.56 in the WRF QPE experiment including the assimilation of French radar data.

Keywords: short-range forecasting, radar, mesoscale convection, reflectivity operator, Z-R relationship

1. Introduction

Due to its high variability in space and time, precipitation strongly influences the spatial and temporal patterns of hydrologic catchment response, especially when threshold-dominated processes such as infiltration, overland flow or erosion are involved (Winchell et al., 1998). Two strong flood events in 2013, one caused by several days of heavy rain in Central Europe in May and June as well as another one in September along the Colorado Front Range, where at certain stations almost the whole annual precipitation fell within 1 week (Hamill, 2014; Schwartz, 2014), demonstrated in a striking way the direct impact of precipitation on human economy and life. Thus, estimating and forecasting the temporal and spatial distribution of precipitation is important for many end users, for example, tourism, agriculture and flood forecasting centres applying hydrological models with precipitation as the major input variable. Correct quantitative precipitation estimation (QPE) and forecasting (QPF) are therefore among the most important tasks in atmospheric sciences.

*Corresponding author.
email: hans-stefan.bauer@uni-hohenheim.de

Citation: Tellus A 2015, **67**, 25047, http://dx.doi.org/10.3402/tellusa.v67.25047

Historically, rainfall was only observed at points in space with rain gauges. To retrieve spatial patterns, various interpolation techniques of different complexity were developed, ranging from Thiessen Polygons (Thiessen, 1911) or Inverse Distance Weighting (Shepard, 1968) to more advanced geostatistical approaches such as Kriging (e.g. Dorninger et al., 2008) or the Vienna Enhanced Resolution Analysis (VERA; Steinacker et al., 2006). However, even for medium rainfall intensities, gauge correlations may drop as low as 0.4 at distances of only 6 km from each other (Moreau et al., 2009). This effect is even more pronounced for convective rainfall due to the higher spatial heterogeneity and intensity. Therefore, gauge interpolation techniques are only adequate for large-scale applications.

To overcome the problem of spatial non-representativeness of rain gauges, weather radar with its high temporal and spatial resolution as complementary data source has been investigated in a multitude of initiatives such as, for example, AQUARADAR (Troemel et al., 2009), COST 717 (Rossa et al., 2005) or RADOLAN (Bartels, 2004). Nevertheless, there are strong limitations on any combination of radar and rain gauge observations. This is mainly due to the indirect nature of radar measurements, the non-agreement of radar and rain gauge sampling location and volumes as well as radar error sources such as path attenuation, ground clutter, beam blockage, anomalous beam propagation, bright band effects and unknown radar Z-R relationships (e.g. Sauvageot, 1992; Villarini and Krajewski, 2010). To overcome this limitation, research has focused on the conceptual description and correction of radar errors (e.g. Germann et al., 2009; Rossa et al., 2009), the investigation of the usefulness of additional observations on the space-time structure of rainfall (e.g. Lee and Zawadzki, 2005; Lee et al., 2007; Berenguer and Zawadzki, 2008; Niu et al., 2010; Tapiador et al., 2010) and a detailed understanding of radar signals and their interaction with hydrometeors to retrieve their microphysical properties (e.g. Dotzek and Beheng, 2001; Brandes et al., 2004a, 2004b; Peters et al., 2005; Cao et al., 2008).

Despite strong research activities and considerable achievements, rainfall estimation based on radar and rain gauges is still not optimal and is not expected to exceed a certain quality limit. The reason is that the atmosphere will probably never be scanned completely and errors in the measurement process remain, so that unobserved points always exist where interpolation or estimation is necessary.

Atmospheric modelling has the potential to complement the observation-based approaches. It produces consistent states with respect to the 3D thermodynamic fields, cloud water, cloud ice and precipitation. At horizontal resolutions coarser than about 4 km, deep convection requires to be parameterised, inducing systematic errors in the simulation of clouds and especially precipitation (Schwitalla et al., 2008, 2011; Wulfmeyer et al., 2008, 2011; Rotach et al., 2009). In recent years, with increasing computer performance, research centres followed by several forecast centres began to operate their models on the so-called convection-permitting scale with horizontal resolutions of 3 km or less, where a parameterisation of deep convection is no longer necessary (e.g. Steppeler et al., 2003; Saito et al., 2007; Lean et al., 2008; Seity et al., 2011). All model systems contain parameterisations and a detailed description of land-surface properties including soil (Milovac et al., 2014a, 2014b) and vegetation suitable for the fine resolution.

For this study, the Weather Research and Forecasting (WRF) model (Skamarock et al., 2008) is applied. We operated the model system successfully for case studies during the World Weather Research Programme (WWRP) Research and Development Project (RDP) COPS[1] (Wulfmeyer et al., 2011) and the Forecast Demonstration Project (FDP) D-PHASE[2] (Rotach et al., 2009) that were carried out in parallel and coordinated with each other. In a case study of Schwitalla et al. (2011), WRF was superior to other models that participated in the projects. Another important finding of the intercomparisons during D-PHASE was that models operated on the convection-permitting scale clearly outperformed models with coarser resolution (Weusthoff et al., 2010; Bauer et al., 2011).

Data assimilation merges a priori information about the state of a dynamic system with observations. This provides an optimal estimate of the current condition of the system (analysis). A prerequisite for excellent simulations is an as-best-as-possible analysis including QPE that is consistent with model physics as well as with observations. This is especially important for clouds, precipitation and small-scale dynamics. Otherwise, the quality of the forecast will degrade rapidly due to model spin-up.

So far, inconsistent analyses prohibited the use of numerical models for nowcasting applications. However, recent skill score analyses demonstrate that convection-permitting mesoscale models start to outperform extrapolation-based nowcasting methods at forecast lead times of 2–3 hours (Tafferner et al., 2008; Kober et al., 2010). With an accurate analysis, the model acts as a dynamically and physically consistent rainfall interpolator in combination with multi-sensor observations. Compared to radar-QPE only relying on low-level precipitation scans, model-based QPE makes use of the full 3D radar observations. Thus, combining models and new observations with

[1]COPS: Convective and Orographically induced Precipitation Study.

[2]D-PHASE: Demonstration of Probabilistic Hydrological and Atmospheric Simulation of flood events in the Alpine region.

DA has the potential to provide QPE in a quality and resolution equal or better than merely observation-based approaches.

The use of atmospheric models and data assimilation for QPE is a relatively new subject. Zupanski et al. (2011) successfully applied a prototype ensemble assimilation system and a cloud resolving WRF model to downscale observations from the Global Precipitation Measurement mission (Smith et al., 2007) to finer resolution. In the current work the performance of QPE, done with a high-resolution WRF simulation including data assimilation, will be investigated. In contrast to operational QPF, performed with free forecasts over the forecast range from one analysis, the presented methodology is to our knowledge the first study of this kind in Europe. To compare our approach with currently applied QPF efforts, we include a downscaling from the ECMWF operational analysis into this study.

Particularly, we are addressing the following scientific questions:

- How accurate is the downscaling of the operational ECMWF analysis with WRF?
- How successful is the developed model-based QPE approach in representing the large-scale evolution of precipitation and what in particular is the benefit of the assimilation of 3D radar data?
- Is the developed system successful in improving mesoscale precipitation fields when compared to radar?
- What are the most important processes influencing the performance of the model-based QPE system?
- How can the system be extended and optimised for future applications?

The publication is structured as follows. In Section 2, the setup of WRF and the simulation strategy are briefly described. Furthermore, the observations assimilated into the WRF data assimilation system and those used for verification are introduced. Section 3 describes the synoptic situation of the case study for which the performance of the model-based QPE is investigated. In Section 4, the results of the comparisons of three model simulations are presented. Finally, Section 5 summarises the results, discusses the scientific questions and provides a brief outlook to future activities.

2. Data and Methodology

2.1. Model setup and data assimilation

The applied WRF-ARW model (version 3.5.1) provides a variety of physical options with different complexity ranging from simple schemes for coarse resolution simulations to sophisticated ones for high-resolution applications on the convection-permitting scale. For our experiments, WRF was run with a horizontal resolution of 3 km in a large European domain of 681×692 grid points and 57 vertical levels (Fig. 1). The simulations were driven by the ECMWF operational analysis available every 6 hours with a horizontal resolution of 0.125° (approximately 15 km).

The configuration of the WRF model physics is summarised in Table 1. Due to the high resolution of 3 km, the parameterisation of deep convection is omitted. The selected domain configuration was successfully tested in earlier studies of Schwitalla et al. (2011) and Schwitalla and Wulfmeyer (2014). To include the interaction with the land surface in a realistic way, WRF was coupled with the flexible NOAH-MP model with switchable physics options (Niu et al., 2011). Cloud microphysics is described with a sophisticated 2-moment scheme (Morrison et al., 2009). A stand-alone shallow convection scheme (Hong et al., 2013), introduced in model version 3.5.1, was switched on. It increases the vertical mixing of moisture in the non-precipitating convective boundary layer and is suggested for resolutions down to 1 km horizontal resolution.

In order to force the model to the observed state, it is necessary to merge a model background field (from an earlier forecast) with newly obtained observations using a data assimilation system. The resulting analysis constitutes the best compromise between the model representation and observations. We selected the three-dimensional variational assimilation (3DVAR) method available for the WRF system (Barker et al., 2004, 2012). The aim of variational data assimilation is to find the best least-square fit between a background field $\mathbf{x}_\mathrm{b}$ and observations $\mathbf{y}_\mathrm{o}$ with an iterative minimisation of a cost function $J(\mathbf{x})$ (Ide et al., 1997)

$$J(\mathbf{x}) = \frac{1}{2}(\mathbf{x}-\mathbf{x}_\mathrm{b})^T \boldsymbol{B}^{-1}(\mathbf{x}-\mathbf{x}_\mathrm{b}) + \frac{1}{2}(\mathbf{y}-\mathbf{y_0})^T \mathbf{R}^{-1}(\mathbf{y}-\mathbf{y}_0). \quad (1)$$

Here $\mathbf{R}$ is the observation-error covariance matrix which consists of observation and representativeness errors. $\mathbf{B}$ denotes the background-error covariance matrix describing the background forecast error. The observation is represented by $\mathbf{y}_0$ and the modelled observation by $\mathbf{y}=\mathbf{H}(\mathbf{x})$. $\mathbf{H}$ is the forward or observation operator, transforming the model variables to the observed quantities at the observation location. For the derivation of the $\mathbf{B}$-matrix, the National Meteorological Center (NMC) method (Parrish and Derber, 1992) for a 1 month period in July 2012 was applied to take into account the strongest variability of the atmosphere in the convective season. The method estimates $\mathbf{B}$ from forecast differences valid at the same time

$$\mathbf{B} = (\mathbf{x}_{t+24h} - \mathbf{x}_{t+12h})(\mathbf{x}_{t+24h} - \mathbf{x}_{t+12h})^T, \quad (2)$$

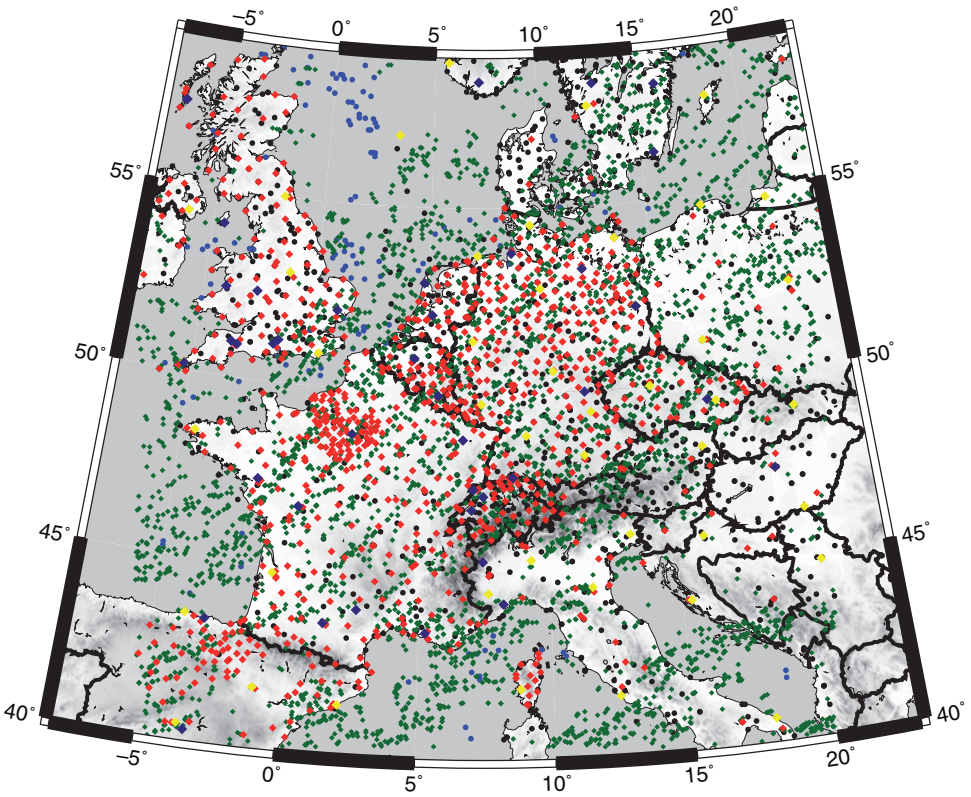

Fig. 1. Model domain, observation types, and their locations for the assimilation at 00 UTC, 26 September 2012. Black = Surface stations (SYNOP + Metar), blue = ship observations (SHIP), green = aircraft observations and atmospheric motion vectors from satellite (AMDAR + SATOB), red = GPS zenith total delay, yellow = radiosondes (TEMP) and brown = wind profiler.

where 12 and 24 hour forecasts were selected to ensure that the calculation of the covariance terms is influenced only minimally by the model spin-up. Due to its size, the calculation, let alone the storage of **B** is unfeasible, and so variable transformations are applied to reduce the number of non-zero elements of **B**. More details about the transformations and the method used to do the iterative minimisation can be found in Schwitalla et al. (2011) and Barker et al. (2004). The performance of the 3DVAR system has been investigated in several publications (e.g. Sugimoto et al., 2009; Schwitalla et al., 2011; Ablash et al., 2012; Liu et al., 2013a, 2013b; Schwitalla and Wulfmeyer, 2014). It provides reliable results down to the convection-permitting scale applied in this study.

Table 1. Parameterisation schemes applied for the WRF QPE experiment

Physics	Applied scheme
Long wave radiation	RRTMG (Iacono et al., 2008)
Short wave radiation	RRTMG (Iacono et al., 2008)
Deep convection	Simulated explicitly
Shallow convection	GRIMS (Hong et al., 2013)
Cloud microphysics	Morrison 2-moment (Morrison et al., 2009)
Planetary boundary layer (turbulence)	YSU (Hong et al., 2006)
Land surface scheme	Noah-MP (Niu et al., 2011)

In the WRF data assimilation system (WRFDA) several observations are included, as e.g. Global Positioning System Zenith Total Delay (GPS ZTD), observations from surface weather stations (SYNOP), ship measurements, airports and aircraft measurements, radiosondes and atmospheric motion vectors. Figure 1 provides the model domain and the observations assimilated at 00 UTC, 26 September 2012.

The observations were pre-processed in the WRFDA system with the OBSPROC package. It provides different error values for the different variables depending on the observing platform. These values were derived from US Air Force Weather Agency (AFWA) statistics. For instance, temperature and dew point errors vary between 1 and 2°C, wind speed errors vary between 1 and 4.5 m/s depending on height and platform and wind direction error was set to 5°. We did not use the new capability to assimilate wind direction and wind velocity separately from each other (Huang et al., 2013). The observation error covariance matrix **R** in the

3DVAR system is a diagonal matrix containing the reciprocals of the variances of the errors in its main diagonal. After the first calculation of the observed quantities from the model variables, a quality check of the new data is done to reject measurements that are too far away from the model background. They would constrict the minimisation of the cost function. More details about the observation preprocessing can be found in Schwitalla et al. (2011).

Radar reflectivities as well as radial velocities from the Doppler precipitation radar systems of the French ARAMIS network (Tabary et al., 2006) were assimilated. In total, data from 24 radars were included. Nineteen radars use C-band transmitters with a frequency of 5.6 GHz, while five radars use S-band transmitters with a frequency of 2.8 GHz. Data were available every 15 min with a resolution of 1 km. The radar antenna is rotatable so that different antenna azimuths and elevations can be scanned. Typical azimuth increments are 1° and the elevation angle increases with height. For C-Band radars, a wavelength of $\lambda = 5.3$ cm and a pulse repetition frequency (PRF) of 600 Hz is applied. The use of a triple PRF scheme allows unambiguous velocities of about 60 m/s at a maximum range of 250 km (Tahanout et al., 2009). Figure 2 shows the coverage of the French radar systems. The data were provided on a 1×1 km grid for each elevation between 0.4° and 17°. The data were thinned and filtered by a median filter on a 10×10 km grid applying the algorithm described in Montmerle and Faccani (2009). In a first quality control, too noisy observations (e.g. clutter, beam blockage) were removed. Due to beam broadening, the radial velocity error varies with measurement range and can be as large as 5 m/s (Montmerle and Faccani, 2009). The observation error for reflectivities was set to 5 dBZ. Observations were considered for assimilation, when the absolute observation-minus-background difference was smaller than 15 dBZ for reflectivities and smaller than three times the observation error for radial velocities.

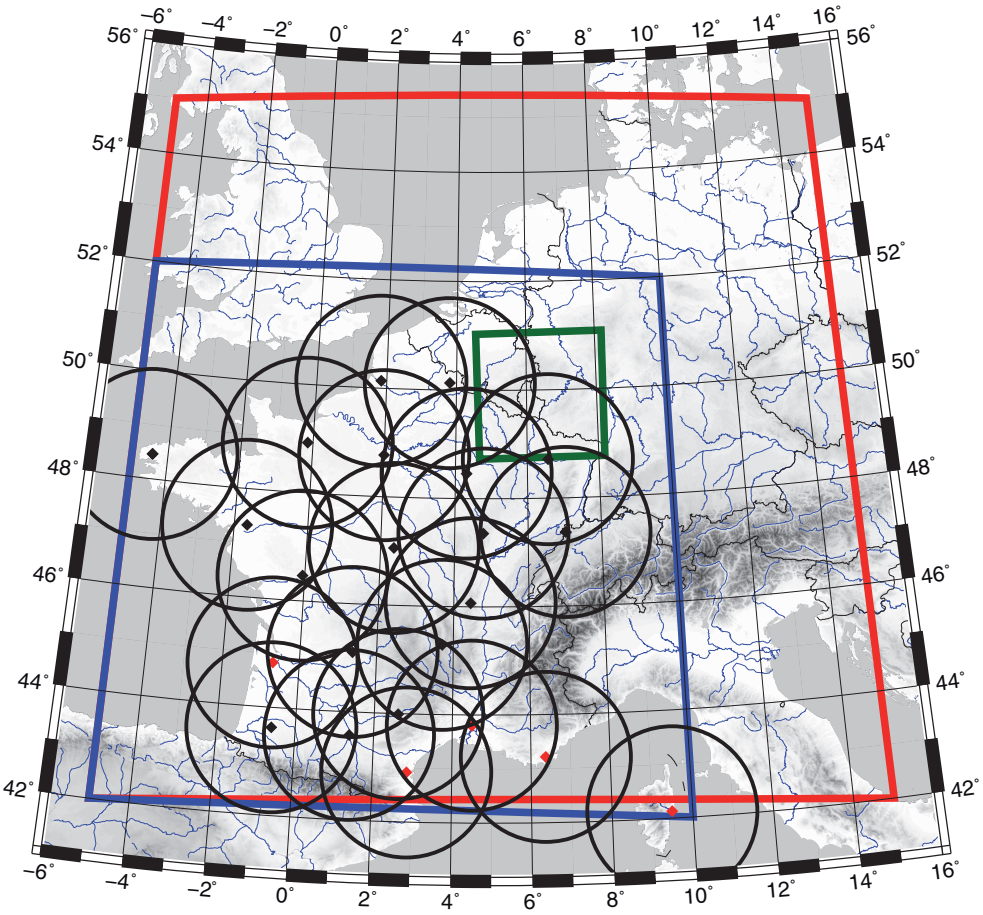

Fig. 2. Coverage of the different radar systems applied in the WRF experiment. The radar circles of the French systems have a radius of approx. 160 km; the red dots represent S-band radar systems and the black dots C-band radars. The red frame marks the verification domain for the qualitative verification, the green frame shows the small verification domain centred over Luxembourg and the blue frame marks the verification domain for the investigation of the performance of the radar data assimilation.

To assimilate radar radial velocities, the three model wind components u, v and w have to be projected to the radar beam position. In the WRF model, this is done following Xiao and Sun (2007) with

$$v_r = \frac{x - x_i}{r_i} \cdot u + \frac{y - y_i}{r_i} \cdot v + \frac{z - z_i}{r_i} \cdot (w - v_T). \quad (3)$$

Here x, y and z denotes the radar location, x_i, y_i and z_i are the locations of the radar observation and r_i is the distance between the radar and the observation relative to the centre of the Earth. v_T is the 'terminal velocity' describing the fall speed of rain particles in the model. Due to the beam broadening and the corresponding difficulties in defining distinct observation locations, observations above 10 km were not assimilated.

For the assimilation of radar reflectivity in the WRF 3DVAR, the reflectivity forward operator of Sun and Crook (1997) is applied. It considers the rain water mixing ratio and is defined by

$$Z = 43.1 + 17.5 \log\left(\frac{q_r \rho_{air}}{kgm^{-3}}\right) [dBZ], \quad (4)$$

where Z is the reflectivity, q_r the rain water mixing ratio ($kgkg^{-1}$) and ρ_{air} the air density (kgm^{-3}).

A drawback of eq. (4) is that it assumes that only liquid hydrometeors are present (Dudhia, 1989). This is easily violated in midlatitude precipitation systems since also hail, graupel and snow are produced and cold rain processes as, for example, the Bergeron–Findeisen process are actively involved in the development of precipitation. This weakness was considered for the assimilation in a way that reflectivities above 3500 m and values larger than 55 dBZ were discarded. Also reflectivities smaller than 0 dBZ were neglected.

Another disadvantage is that this warm rain scheme is quite simple compared to the two-moment scheme selected for the free forecasts. This leads to imbalances between the analysis and the subsequent forecast due to different thermodynamics. Unfortunately no other microphysics scheme is available for the WRF assimilation system at the moment. Further details of the pre-processing and assimilation of radar data can be found in Schwitalla and Wulfmeyer (2014).

Due to the large number of measurements, radar data is only processed at analysis time. For the other observations, the time window is ± 30 min around analysis time. In total, about 5000 conventional observations and 40 000 radar observations were included into the assimilation.

It is important to note that ground-based precipitation observations are not assimilated. Main reasons are that simulated precipitation is a result of a long chain of processes that cannot be resolved explicitly. This chain is represented by the cloud microphysics scheme making it difficult to relate the observed precipitation to distinct model variables. Furthermore, its strong dependence to the real surface orography (not equal to the model orography) and its strong spatial heterogeneity aggravate the development of a forward operator. We are aware of experiments using surface-based gauge data in the assimilation (e.g. Lopez, 2013), but such an approach is not possible for the WRF 3DVAR system and therefore not further discussed here.

We operated the model and assimilation system in a 1-hour Rapid-Update Cycle (RUC, see Fig. 3). In this RUC setup, 1-hour forecasts were started each hour from a 3DVAR analysis. The precipitation fields provided by the short forecasts were then used as a quantitative precipitation estimate.

2.2. *Performed experiments*

Our CONTROL simulation is a downscaling of the operational ECMWF analysis to a horizontal resolution of 3 km. This simulation serves as a reference for all our model-based QPE experiments, since it mimics the QPF efforts done at operational weather centres when no re-assimilation of the observations is done during the nesting to the finer resolution. With the QPE approach described above, two more experiments are included in the investigation. The ASSIM_NORAD experiment assimilates all available observations apart from volume radar data (reflectivity and radial velocity). The ASSIM_ALL experiment in addition includes the assimilation of radar data. All three experiments are initialised at 00 UTC, 26 September 2012 and run until 12 UTC, 27 September 2012. While the CONTROL simulation is a free forecast over the 36 hours, the other experiments are rows of 1-hour forecasts, each initialised by a 3DVAR.

2.3. *Verification procedure and applied observations*

Our verification strategy consists of two steps. First, the general performance of the developed system was investigated. Here, we answer the question of whether this setup leads to an improvement over the downscaling from the ECMWF analysis. As we operate the system with a high horizontal resolution of 3 km, the calculation of standard verification scores alone carries the risk of masking improvements with the so-called double-penalty problem (Nurmi, 2003). Furthermore, it is the intention to verify the capability of the simulations to represent the changing synoptic situation on a larger spatial scale over a certain period of time. Here, we are interested in both the spatial structures as well as the temporal evolution. Therefore, derived radar products from the German Weather Service (DWD) and Météo France, covering almost the

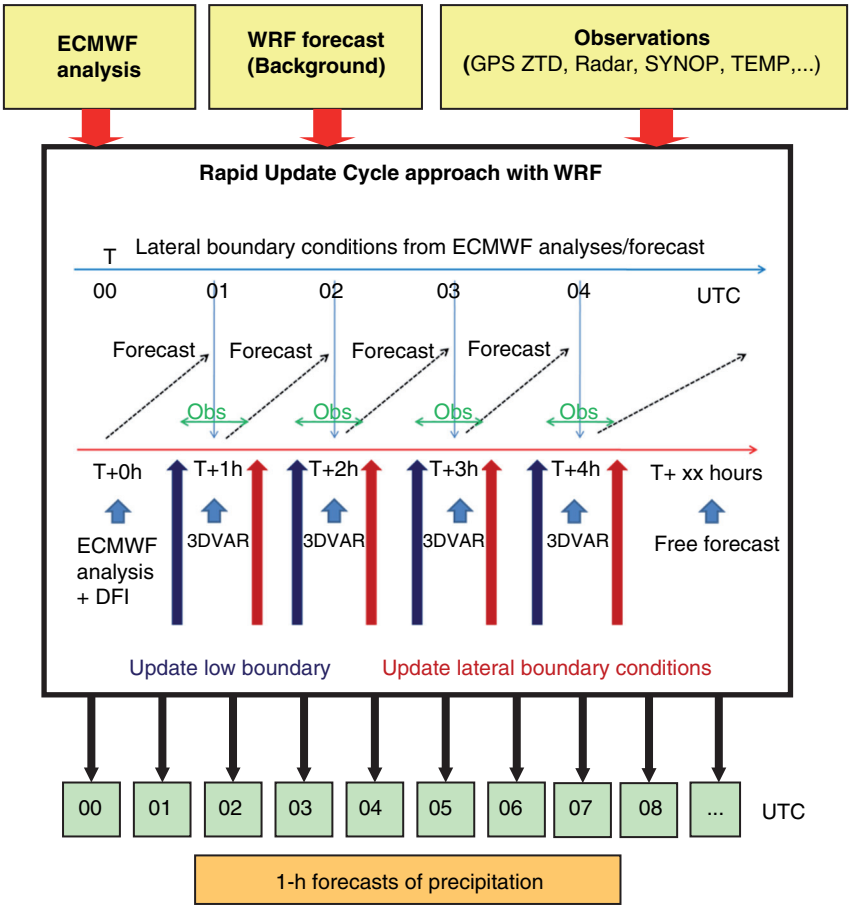

Fig. 3. Sketch illustrating the WRF QPE approach.

entire model domain, are selected for the overall verification of the case study. They are better suited than rain gauge data to derive the synoptic structures and their temporal developments.

RADOLAN ('RADar-OnLine-ANeichung', Bartels, 2004) is an operational merging procedure of radar data from the 16 radar systems of DWD and gauge measurements and combines the advantages of the two measuring principles in one data set. Here we focused on two operationally derived products: The RADOLAN RX is the composite product of uncorrected reflectivity at single time steps and the lowest elevation. The German composite has a temporal resolution of 5 min and a spatial resolution of 1 km^2 over a domain of 900×900 km^2. The French reflectivity composite product is generated every 5 min at the horizontal resolution of 1 km^2 over a domain of 1536×1536 km^2. For each pixel, the reflectivity value is taken as the maximum value of the reflectivities measured by the radars that cover the pixel. For the verification, the RX product was merged with the reflectivity composite from Météo France into one product. During the merging of the two products, the data were interpolated to 3 km, corresponding to the model resolution.

Furthermore, the RADOLAN RW product was selected, containing hourly accumulated precipitation amounts derived from reflectivity with the application of a quality control algorithm (clutter, shading) and a Z-R relation to derive intensity of precipitation from the reflectivity. It is calibrated to hourly accumulated measurements from automatic precipitation stations (Bartels et al., 2005). It is available at 1 km horizontal resolution and for a fairer comparison also interpolated to the coarser model resolution.

The configuration with no radar data assimilated over Germany was applied to investigate whether an upwind assimilation of radar data is capable of changing the atmospheric structure in a way that leads to improved representation of precipitation downwind where no radar data were assimilated.

While the hourly precipitation amount is part of the results of the 1-hour forecasts, the reflectivity was calculated from the model output as done by the 3DVAR radar forward operator [eq. (4)]. The verification of both variables

provides complementing information. While the reflectivity is calculated at one time step, the hourly accumulated precipitation also contains the temporal evolution of the cloud microphysics during the 1-hour forecast.

This qualitative comparison of reflectivity and precipitation fields is followed by two quantitative verification steps. Since the CAOS project (http://www.caos-project.de) is working in a river catchment in Luxembourg, the average hourly accumulated precipitation for a sub-domain of $250 \times 250\,km^2$ centred on this catchment, is calculated from the model simulations and compared with corresponding averages of observation-based QPE methods from rain gauges and the Wideumont radar from the Royal Meteorological Institute of Belgium (Berne et al., 2005; Goudenhoofdt and Delobbe, 2009). The verification domain is shown as a green rectangle in Fig. 2. In addition, a quantitative comparison of 24-hourly accumulated precipitation over Germany with the DWD REGNIE product is done. REGNIE (REgionalisierung von NIEderschlagsdaten) is a consistent gridded data set of daily precipitation. It is generated from 1500 rain gauge stations interpolated on a $1 \times 1\,km^2$ grid over Germany. During the interpolation, the station elevation and exposition is taken into account. To compare the REGNIE data set with the model results, the observations were interpolated to the model grid with an inverse distance weighted approach. The verification is done for the 24-hourly accumulated precipitation from 06 UTC, 26 September 2012 to 06 UTC, 27 September 2012. Horizontal comparisons for the different simulations are done and a set of verification scores is derived.

The verification is followed by a more detailed investigation of the performance of the assimilation system and here particularly the assimilation of radar data. Our focus was set to France and the most western part of Germany, the region covered by the French radars whose data were assimilated. The domain is marked with a blue rectangle in Fig. 2. It is the aim to derive possible reasons for observed weaknesses of the system and to derive pathways to optimise our procedure. To determine the performance of the radar data assimilation, the 1-hour RUC forecast and the following analysis of the simulations with ASSIM_ALL are compared. Apart from variables directly influenced by the assimilation of radar data, the influence on other model variables is also investigated.

3. Synoptic situation

The performance of model-based QPE is tested for a case study during 26 and 27 September 2012. During both days, the synoptic situation changed significantly from the passage of a frontal system on September 26 to the development of convection in the post-frontal cold air on 27 September 2012.

Figure 4 illustrates the situation on 26 September 2012. On that day a large low pressure system was situated over the British Isles. A corresponding upper level trough extended from the eastern Atlantic far south to the Iberian Peninsula. This configuration left the western part of Europe in a south-southwesterly flow regime. Embedded was a marked quasi-stationary cold front with weak front normal winds that stretched from southern France to Scandinavia and separated warm and moist Mediterranean air to the east from cool Atlantic air to the west. Over the eastern Atlantic, cold air was transported far south. Additionally a wave, which travelled along the frontal zone to the north-northeast, intensified the vertical velocity and precipitation locally. The thermal contrast between the pre- and postfrontal air mass was further intensified by prefrontal low-level advection of warmer and humid Mediterranean air, increasing the efficiency of the precipitation formation and the possibility of embedded convective mesoscale precipitation bands within the stratiform precipitation.

On 27 September 2012, the situation changed considerably as illustrated in Fig. 5. The low pressure system moved to the Northeast and was then located over the Baltic Sea. Most of Germany was passed by the frontal system. Only along the Alpine rim, remnants of the Mediterranean air and relief rainfall were still present. To the rear of the frontal system, cold and unstable air masses spread into Western Europe, preparing the environment for more convective precipitation. Especially in the area of a marked 'trough line' with low-level convergence, ranging from Denmark to northeastern France, an enhancement and band-like organisation of the convective activity was observed. In the satellite image even a small comma-like pattern can be identified over eastern France.

4. Results

4.1. Comparison with RADOLAN radar products

Since a comparison of the whole development during the 2-day case study is beyond the scope of the manuscript, we focus on representative snapshots during the development of the synoptic situation.

For the frontal passage on 26 September 2012, we selected 02 UTC, where the almost closed frontal system stretched from southern France over Western Germany northeastward to the Baltic Sea. Figure 6 compares the WRF derived reflectivity from the CONTROL simulation (upper left panel) with the merged reflectivity product combining Météo France and DWD radar data (upper right panel) and the two simulations ASSIM_NORAD (lower left panel) und ASSIM_ALL (lower right panel).

It can be observed that the structure of the synoptic situation is well captured by the CONTROL simulation.

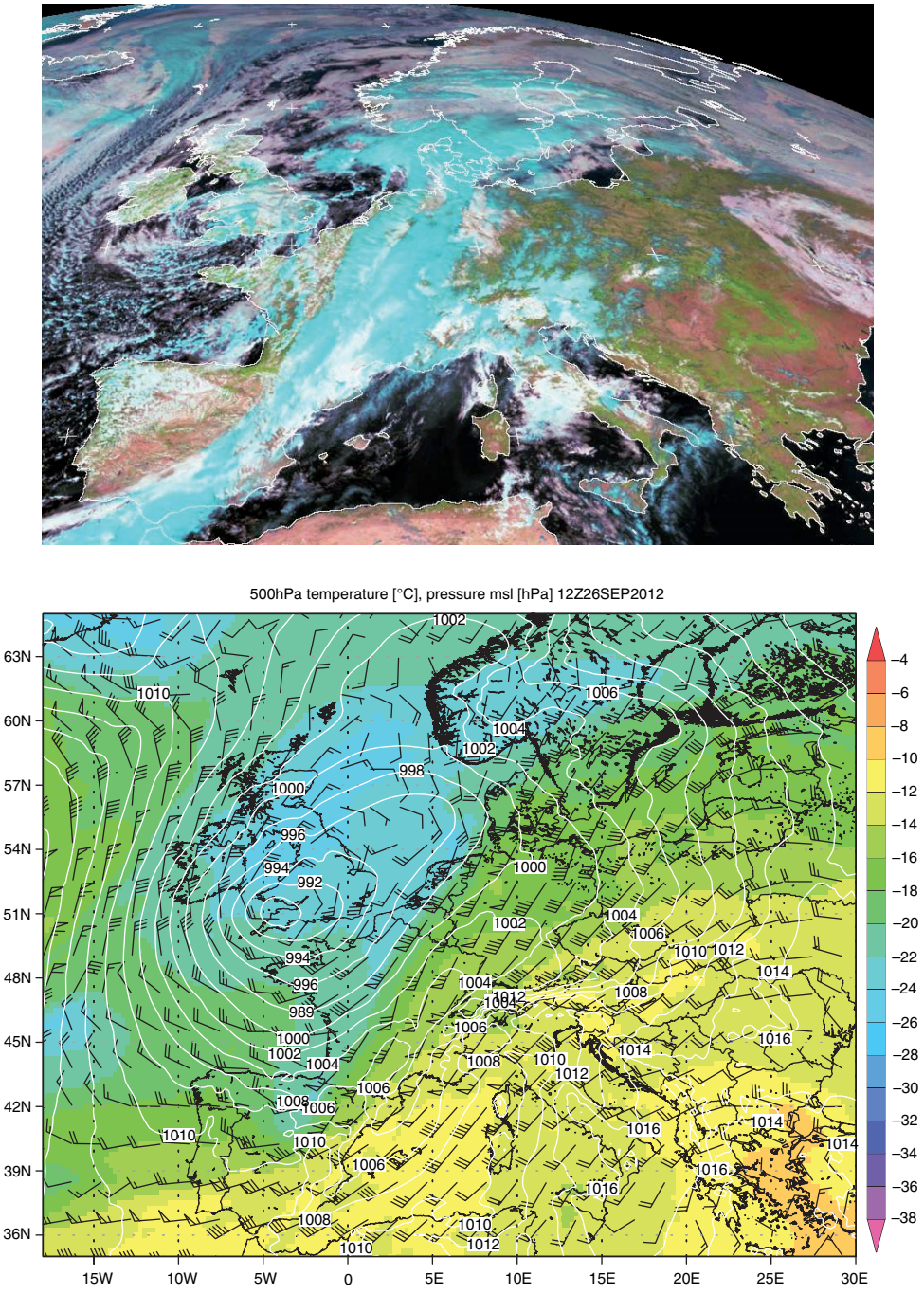

Fig. 4. Synoptic situation at 12 UTC, 26 September 2012. Top: 'Natural colour' composite image of the Meteosat Satellite (Source: NERC satellite receiving station, Dundee University, from http://www.sat.dundee.ac.uk/). Clouds containing ice particles are coloured in cyan. Bottom: ECMWF analysis showing the 500 hPa temperature (°C) (colour) and wind field as well as the mean sea level pressure (hPa) (white contours).

Since the downscaling is done from the operational analysis of ECMWF that includes a global 4DVAR in an assimilation cycle, this is not surprising. Note that the frontal system is reasonably well simulated although radar data is not assimilated in the ECMWF 4DVAR system. Especially over France, it compares well with the radar composite. Due to the coarse horizontal resolution of the driving analysis and varying model physics, differences in detail occur. The front moves too rapidly when compared to the radar observation, and the extension of the front over Northern Germany and

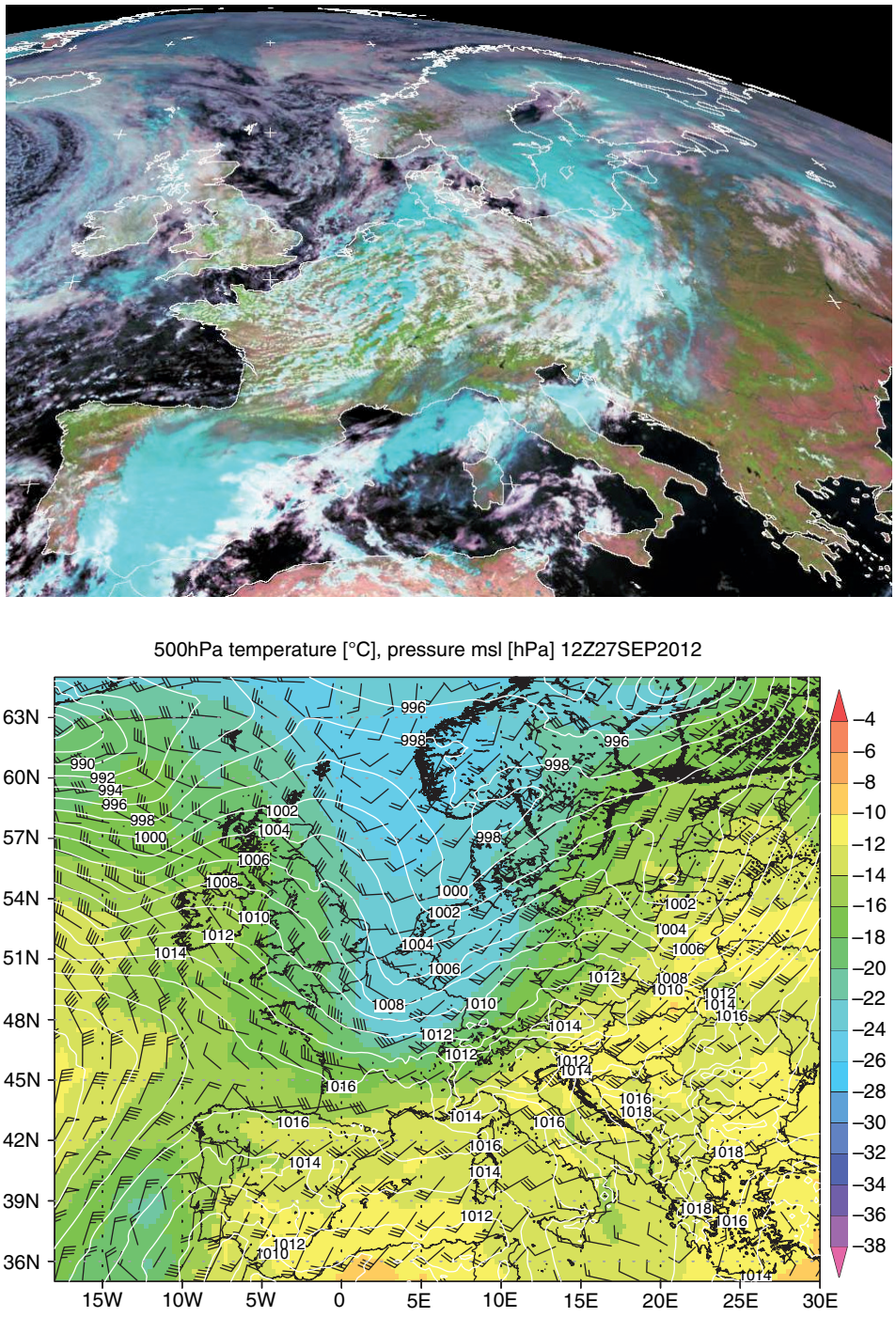

Fig. 5. Same as Fig. 5, but for 12 UTC, 27 September 2012.

the pre-frontal line of convection, stretching from southwest to northeast over Germany, is almost not simulated. Furthermore, the front shows a more diffusive structure as compared to the radar composite. Due to the coarser resolution of the driving analysis and the corresponding spin-up of the post-frontal convection, the convective activity to the rear of the front is not simulated.

In the ASSIM_NORAD simulation, the frontal movement is still too rapid, especially over northern France and Germany. The assimilation leads to an even broader and more diffusive representation of the front compared with the radar composite and the CONTROL simulation. Another obvious change due to the assimilation is that the cellular convection developing in the cold air to the west of the cold

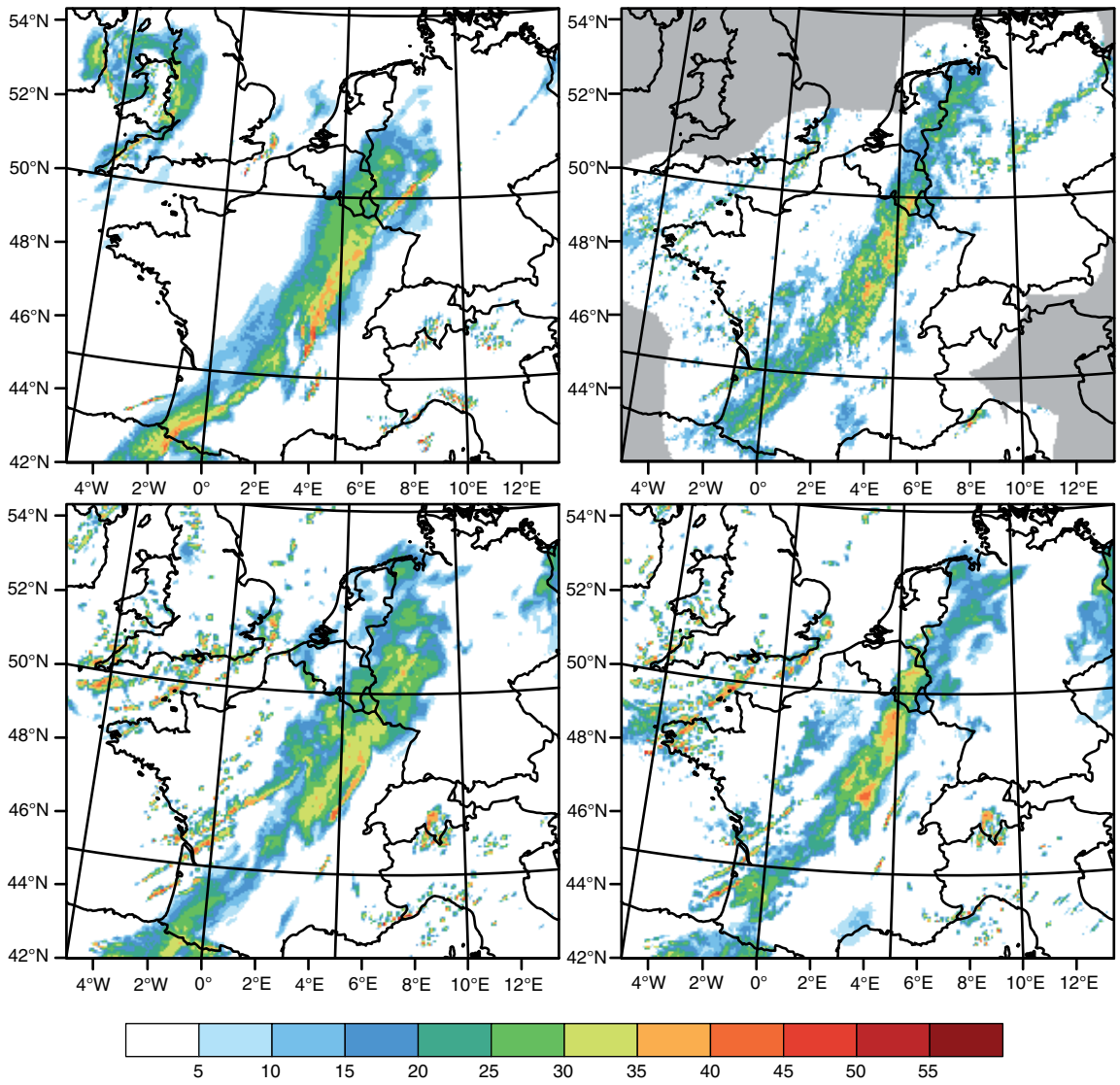

Fig. 6. Comparison of the maximum reflectivity (dBZ) of the WRF CONTROL simulation (top left), the merged reflectivity composite of Météo France and DWD (top right) (areas not covered by radar in grey), the ASSIM_NORAD simulation (bottom left) and the ASSIM_ALL simulation (bottom right) for 02 UTC, 26 September 2012.

front is now represented by the simulation. It is too strong when compared to the radar composite, although the observed organisation into rain bands is seen. The extension of the front over northern Germany is better represented as compared with the CONTROL simulation, but the observed line of convection over Germany is still not simulated.

ASSIM_ALL further improves the situation. Compared with the other two experiments, the too rapid movement of the front is clearly reduced, so that the rain band over France, Belgium and Luxembourg is simulated at the correct location. Only the northern part of the front over Germany is slightly too weak and moves somewhat too rapidly. One reason might be that only radar data from French systems were assimilated. This is also one of the reasons why the reflectivity over the eastern part of the model domain is still simulated and the pre-frontal line of convection, stretching from the front to the northeast, is not captured by the simulation. Nevertheless, the benefit of the radar data assimilation is clearly seen. Aside from the better location, the front is sharpened towards the observation and even the positions of the local intensity maxima correspond to the radar composite. Although still overemphasised, the overestimation of the cellular convection in the cold air to the rear of the front is reduced compared with the ASSIM_NORAD simulation, in better accordance with the radar composite.

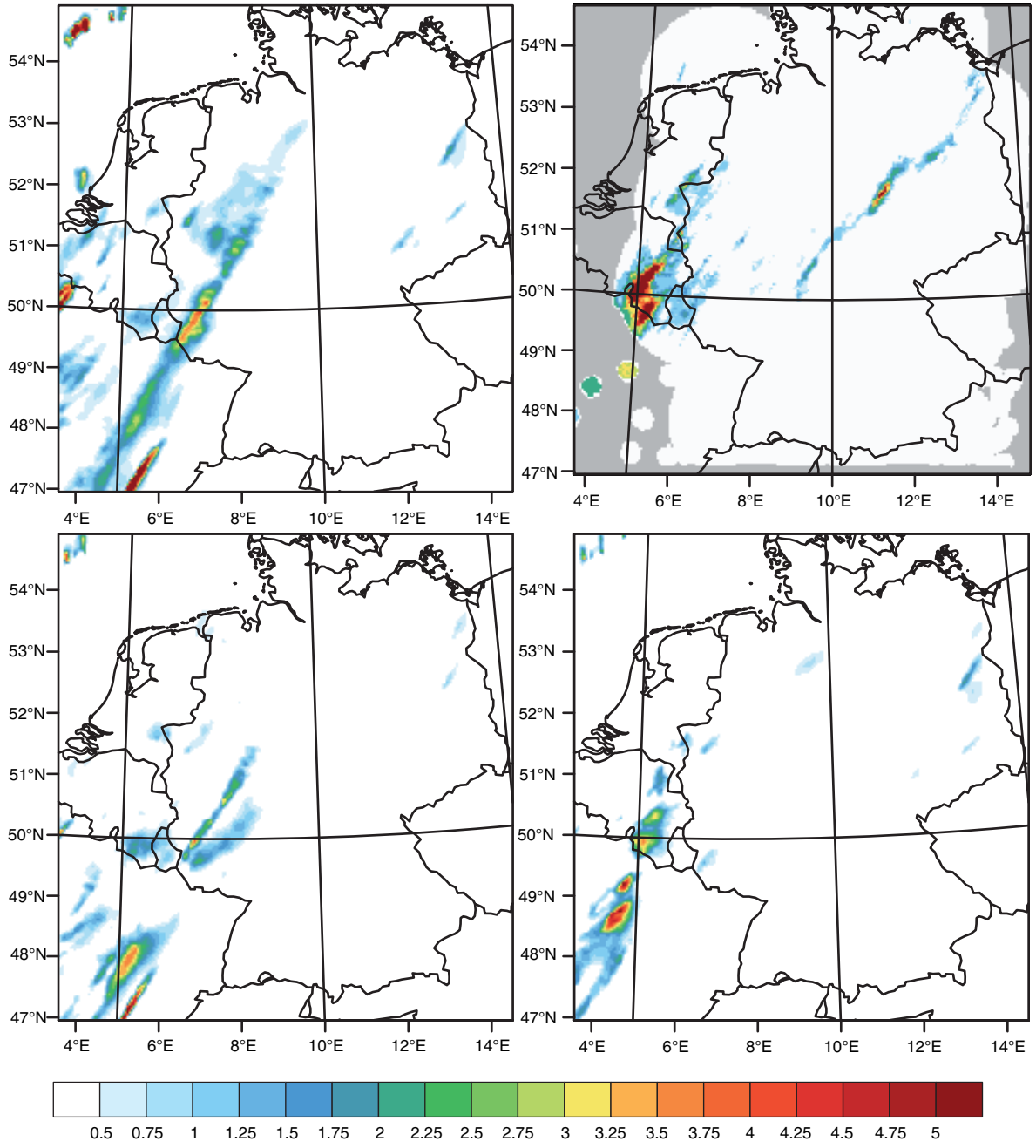

Fig. 7. Comparison of the hourly accumulated precipitation (mm/h) of the WRF CONTROL simulation (upper left), the DWD RADOLAN RW product (upper right), the ASSIM_NORAD simulation (lower left) and the ASSIM_ALL simulation (lower right) for 02 UTC, 26 September 2012.

Figure 7 compares the hourly-accumulated precipitation until 02 UTC, 26 September 2012 of the CONTROL simulation (upper left panel), the RADOLAN RW product (upper right panel), the ASSIM_NORAD simulation (lower left panel) and the ASSIM_ALL simulation (lower right panel). The intensity of precipitation is underestimated in all three simulations. As also suggested by the comparison of reflectivity in Fig. 6, the movement of the frontal rain band is too rapid in CONTROL and ASSIM_NORAD, although the situation is already improved by the assimilation. The representation of precipitation is further improved in the ASSIM_ALL simulation. Although still underestimating the intensity,

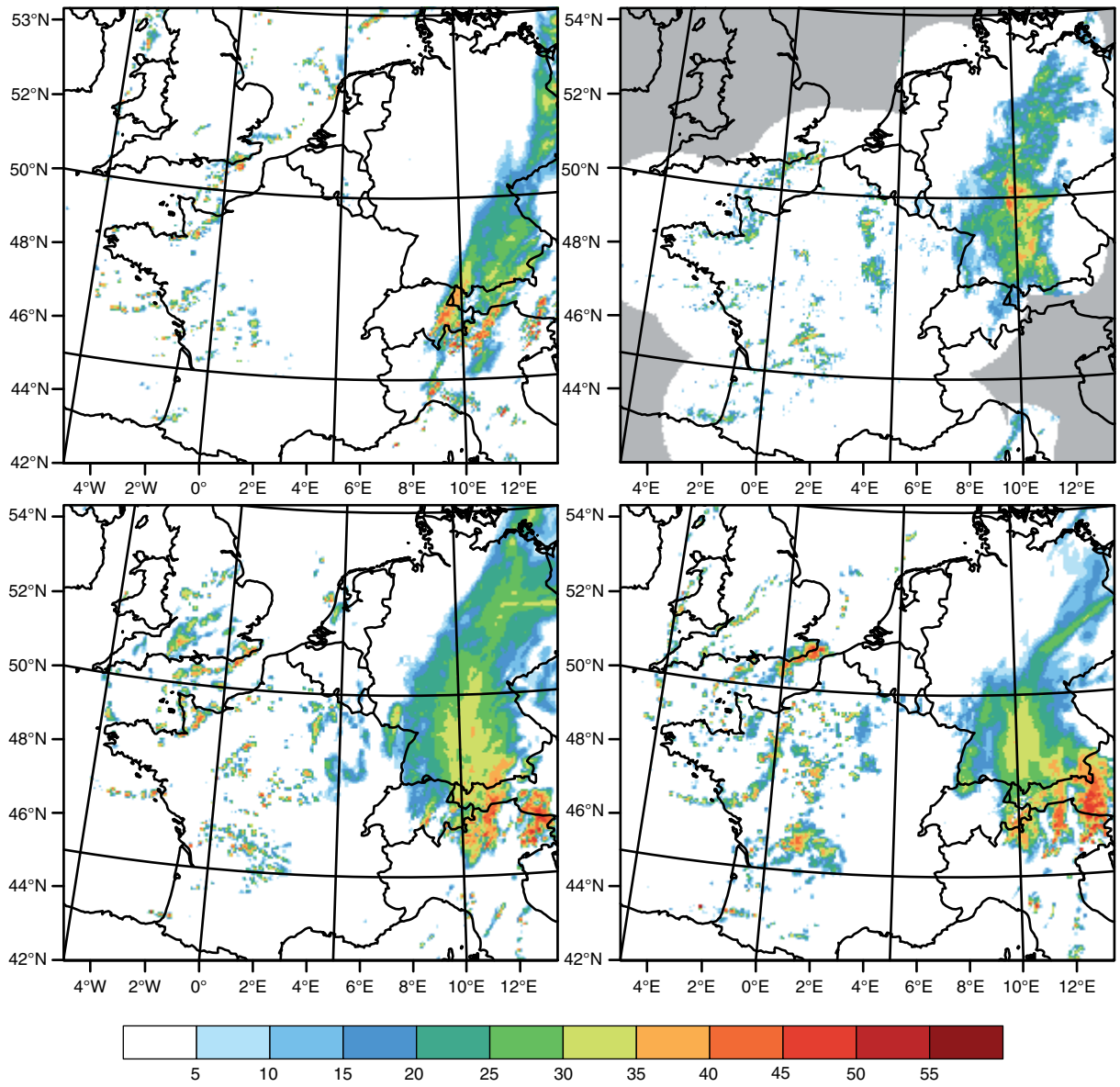

Fig. 8. Same as Fig. 6, but for 01 UTC, 27 September 2012.

the location of precipitation over Belgium and Luxembourg is correctly simulated. As discussed for the reflectivity, none of the simulations are capable of representing the rain band stretching from southwest to northeast over Germany.

During the course of the 26 September, the front continued its passage to the east. At 01 UTC, 27 September 2012, it was located over Germany. Figure 8 compares the three simulations with the merged radar composite in the same way as done for 02 UTC, 26 September 2012. In the CONTROL simulation, the frontal movement is still too rapid. This is true especially for its northern part over Eastern Germany. The re-intensification of the front especially over southern Germany, shown by the merged radar composite, is not simulated by the CONTROL simulation. It continues to weaken and is simulated too far to the east. Although not fully covered by the radar composite, it appears that WRF seems to overestimate the convection over the Alps. In spite of first developments over western France and the British channel, the cellular convection to the rear of the cold front is still underestimated in the CONTROL simulation.

In the ASSIM_NORAD simulation, the location and intensity of the front is much better represented, but it is simulated too diffusive as compared with the radar composite

and the intensity over southern Germany is still slightly underestimated. Over eastern Germany on the other hand, the intensity of the front is overestimated. The convective activity to the rear of the front is increased. Single cells are even stronger than observed by the radar composite. However, the representation is improved compared with the CONTROL simulation. The overestimation of convection over the Alps is even more emphasised in ASSIM_NORAD as compared with CONTROL, indicating that the assimilation deteriorates the situation over the Alps.

In the ASSIM_ALL simulation, the front over southern Germany is narrowed compared with the ASSIM_NORAD simulation in better accordance with the radar composite, but its intensity is still underestimated. To the north, the representation of the front is worse as compared to ASSIM_NORAD. The intensity is reduced too much and the orientation of the rain band is different compared with the radar composite. This may be caused by the missing upwind forcing of the radar data assimilation in the northern part of the model domain due to the westerly flow. The convection over the Alps is again intensified compared with the ASSIM_NORAD simulation. The assimilation of radar data even worsens the situation, indicating a feedback of the assimilation either with the cloud microphysics or the underlying orography that is then further amplified by the assimilation of radar data. The intensity of the cellular convection over France is also stronger than observed. However, in accordance with the radar composite, the location of the cells is more focused to regions where convection was really observed. The existence of a 'comma-shaped' reflectivity pattern over western France south of the Bretagne indicates differences in details of the dynamics as compared to the ASSIM_NORAD simulation. Such band-like structures are, weaker than in ASSIM_ALL, also seen in the merged reflectivity composite.

The tendency to increase the reflectivity where large values are already present was further investigated with the analysis of the sequence of hourly assimilations in the RUC (not shown). It reveals that this exaggeration builds up from hour to hour, leading to the strong convective development over the Alps in Austria not seen in the observation. Since the overestimation was also seen in the CONTROL simulation, the model physics and here especially the cloud microphysics scheme may be responsible for that. Especially in orographic terrain, also the non-resolved part of the convection may contribute to this overestimation. The problem is then enhanced by the assimilation.

Figure 9 compares the hourly accumulated precipitation of the different simulations and the RADOLAN RW product for 01 UTC, 27 September 2012 as done for 02 UTC, 26 September 2012 in Fig. 7. The rapid movement and the distinct underestimation of precipitation in the CONTROL simulation are seen. Furthermore, the development of convection on the rear side of the front over the North Sea starts too early as compared to the RADOLAN observation. The representation is improved in the ASSIM_NORAD simulation where the intensity of precipitation is improved in southern Germany. Nevertheless, it is still too weak and the movement of the front is too rapid. Additional improvement in location and intensity of the front over southern Germany is found in the ASSIM_ALL simulation. This improvement is expected to be a consequence of the radar data assimilation over north-eastern France. The westerly wind transports the influenced environment eastward. However, the widespread and strong precipitation seen in the RADOLAN RW composite is not reproduced by the simulations and precipitation further to the north is also underestimated. On the other hand, precipitation over the Alps is overestimated especially by the ASSIM_ALL simulation. Since this overestimation is clearly weaker in the CONTROL simulation, it suggests that a feedback from the assimilation on the model dynamics is responsible for this artefact. The bow-like structure suggests the development of a small-scale intense low pressure system in the simulation.

During the course of 27 September 2012, the front continued its movement to the east. An unstable maritime air mass in which convective precipitation developed dominated. As a representative snapshot, we investigate the representation of the situation in the different model simulations at 12 UTC, 27 September 2012, where the post-frontal convection was well developed over France, the Benelux countries and the western part of Germany. Figure 10 compares the reflectivity of the simulation and the merged radar composite as done above. The model captures the transition from a southerly dominated flow before the passage of the cold front to a westerly and later north-westerly flow on 27 September 2012. The development of cellular convection in the cold maritime air is represented by all three simulations. The single convective cells are overestimated in size and intensity as compared with the merged radar composite. Since this is the same in all three model simulations, it is not related to the data assimilation. Possible causes are the selected cloud microphysics scheme or that the convection may not be fully resolved at 3 km resolution. Schwitalla et al. (2011) found that the Morrison microphysics scheme tends to produce intense convection with strong vertical velocities and large amounts of graupel, leading to large amounts of rain water mixing ratio and therefore reflectivity in the background field. This may also contribute to the overestimation of precipitation over the Alps.

However, differences in detail between the simulations occur. CONTROL simulates widespread convection of weak and strong intensities. In contrast to the radar composite, no clear organisation of the convection into

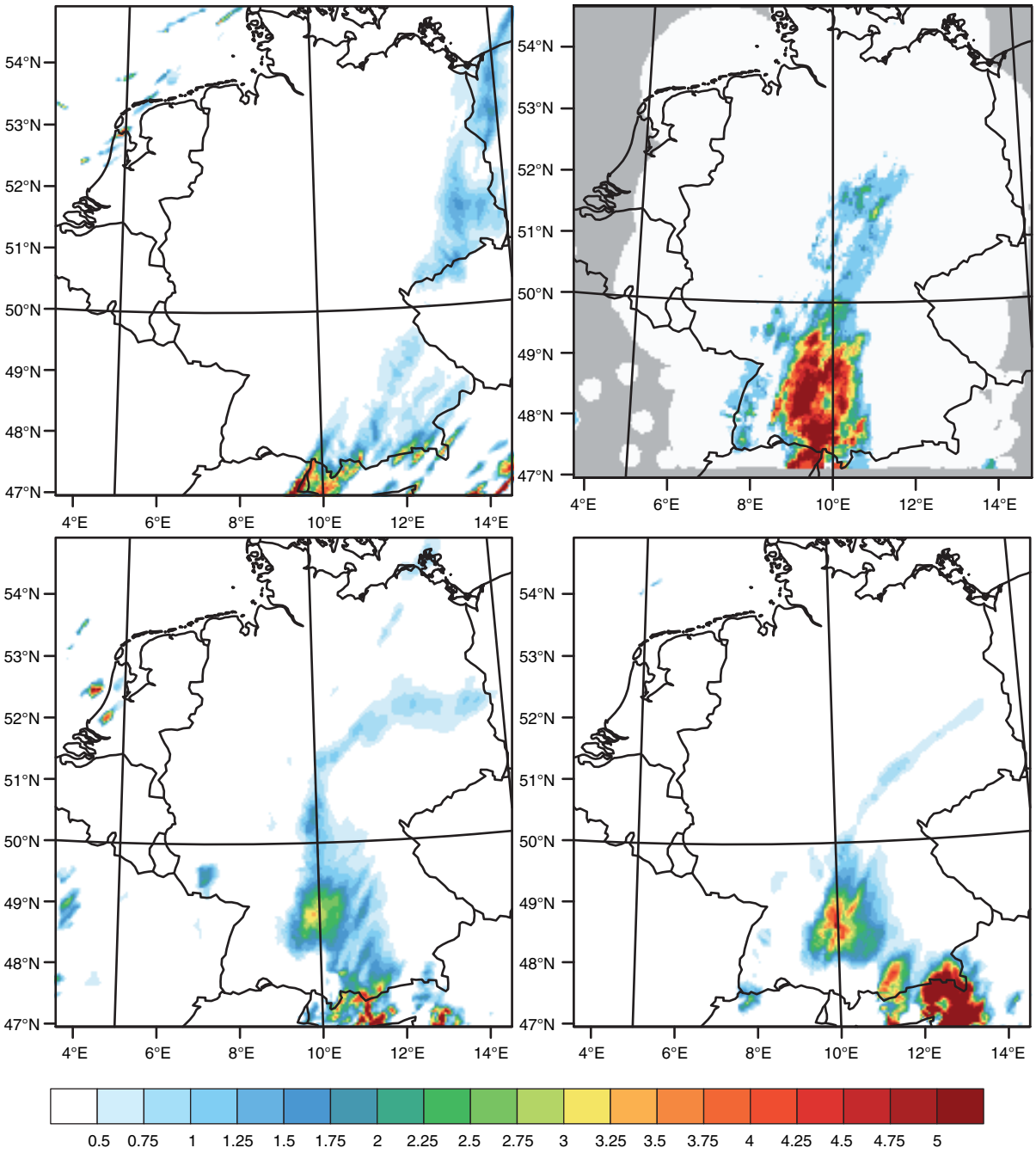

Fig. 9. Same as Fig. 7, but for 01Z, 27 September 2012.

rain bands is seen over northern France and Germany. ASSIM_NORAD reduces the number of cells, especially that of lower intensity. As in the CONTROL run, no clear organisation into rain bands is seen. When radar reflectivity and radial velocity are assimilated (ASSIM_ALL), the organisation of the cells is improved compared with the merged radar composite.

Comparing the simulations with and without assimilation suggests that the assimilation seems to emphasise already existing strong cells in terms of size and intensity, whereas small and weak cells are removed. When radar data is assimilated, this tendency is even enhanced.

Figure 11 compares the hourly accumulated precipitation of the three simulations and the RADOLAN RW composite for 12 UTC, 27 September 2012. The patchy structure of the developing showers is seen in all three simulations. Nevertheless, the model tends to overestimate precipitation. The cells are larger and more intense than observed. This is

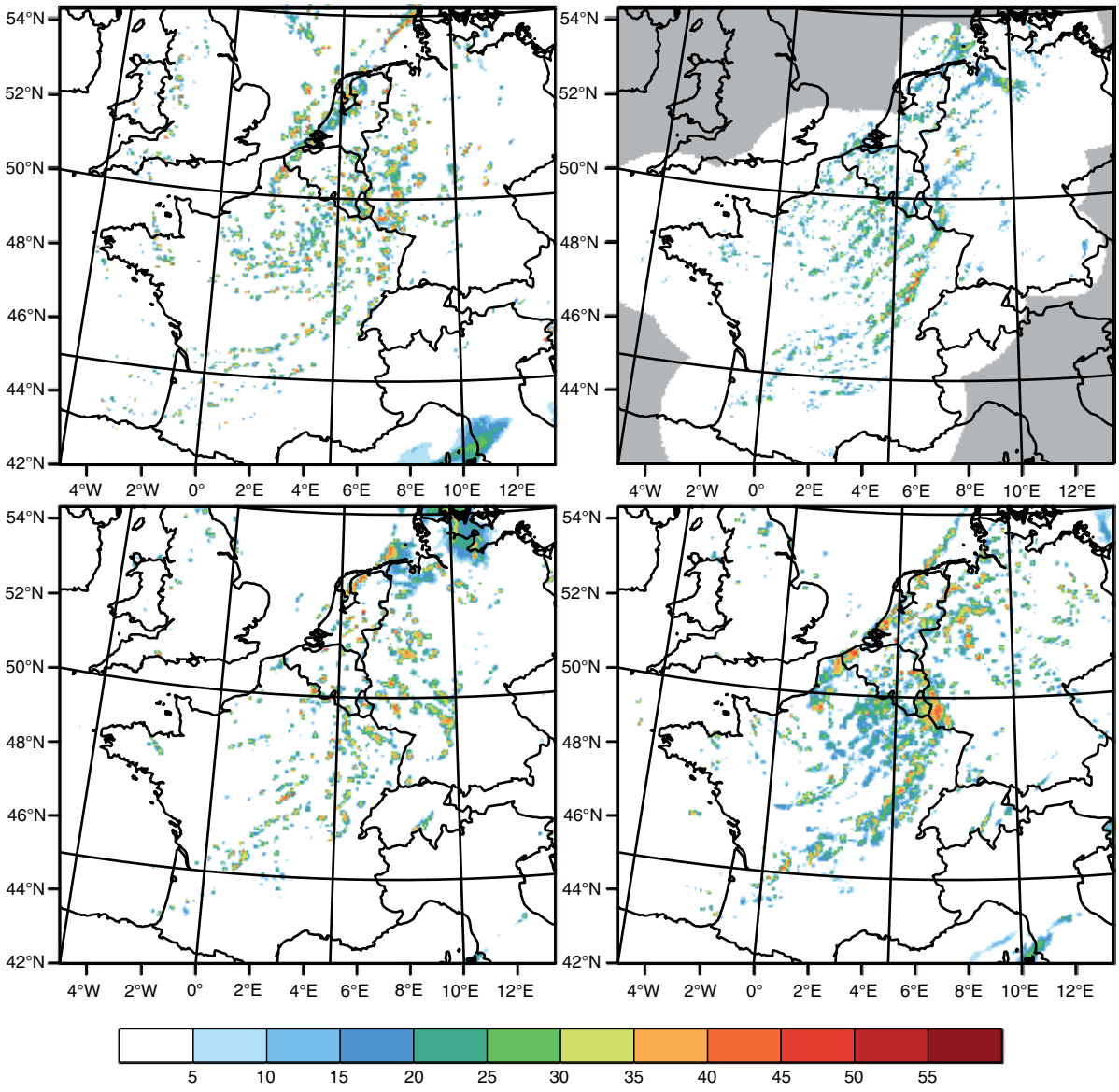

Fig. 10. Same as Fig. 6, but for 12 UTC, 27 September 2012.

apparent even in the CONTROL simulation without data assimilation. Best agreement with RADOLAN RW in terms of the intensity of the precipitation cores is found in the ASSIM_NORAD simulation. The reason might be that conventional observations are assimilated in the whole model domain. With the assimilation of radar data (ASSIM_ALL), the location of the precipitation cores is improved. At the same time, in contrast to RADOLAN RW, the precipitation intensity is increased.

The improvement of the localisation in ASSIM_ALL, when compared to the CONTROL simulation, is not as clearly seen as for the reflectivity. This is caused by the smoothing of the precipitation field due to the accumulation over 1 hour and is also the reason why the band-like structures in the precipitation field are not clearly seen.

4.2. Verification in a small domain centred over Luxembourg

Figure 12 compares the 36-hour time series from 00 UTC, 26 September 2012 until 12 UTC, 27 September 2012 of hourly precipitation spatially averaged over the verification domain marked by the green rectangle in Fig. 2. Shown are the three model simulations and corresponding results calculated from rain gauge data and Wideumont radar observations. As expected the temporal development is

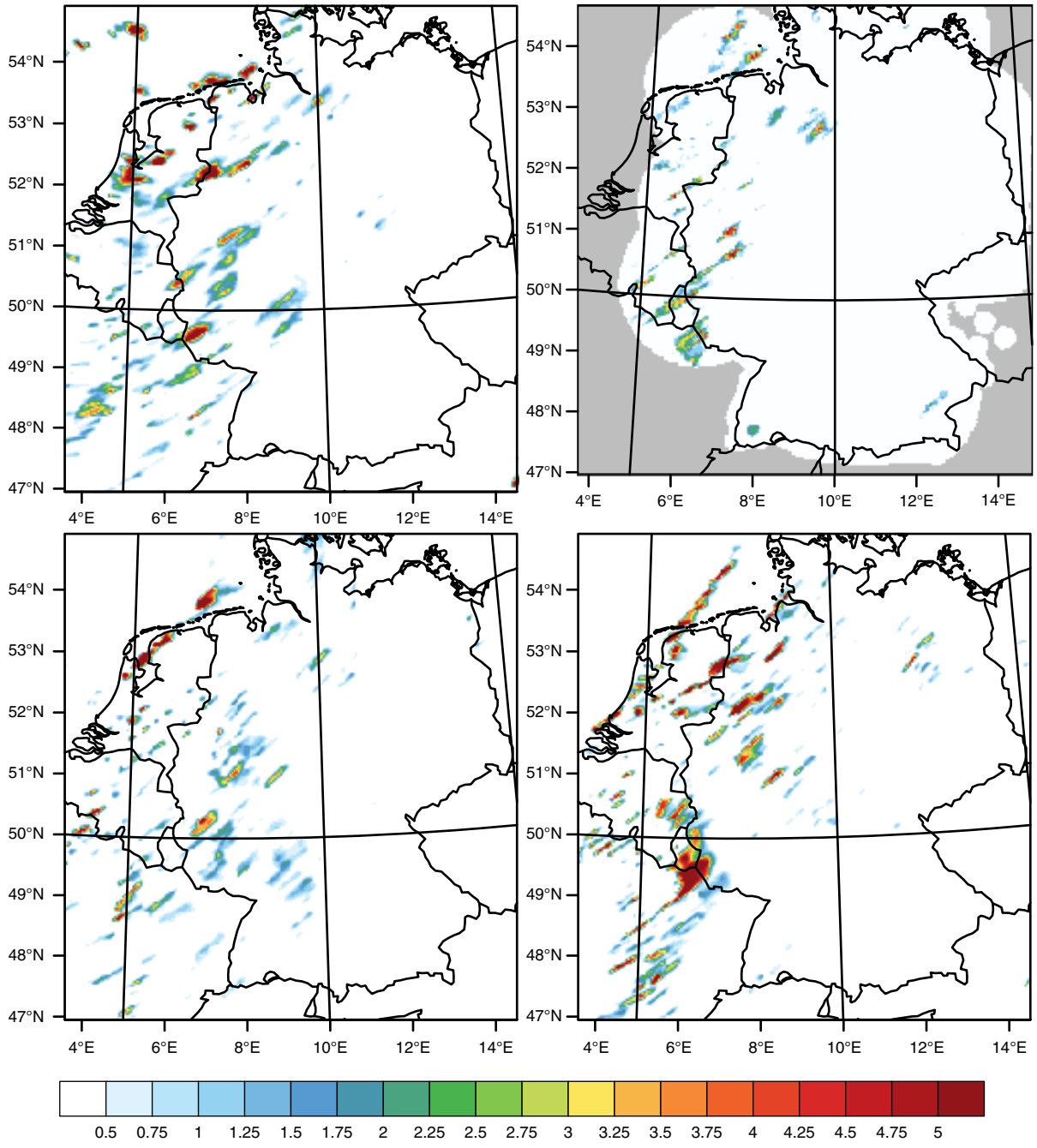

Fig. 11. Same as Fig. 7 but for 12 UTC, 27 September 2012.

similar in all data sets. However, differences between the simulations and observations occur in the temporal evolution and intensity. The strongest representation of the frontal development is found in the ASSIM_NORAD simulation. This is caused by the too broad and diffusive representation. The too rapid movement as compared to the observations is also seen. The CONTROL simulation slightly underestimates the intensity of the front. On the other hand, ASSIM_ALL clearly underestimates the strength of the frontal development. Nevertheless, the correct timing and the narrowing of the front in ASSIM_ALL are apparent. Interestingly, the too rapid movement of the front in CONTROL is not seen, caused by the too broad representation of the front as compared to the radar composite (see Fig. 6).

The second maximum in the early afternoon of 26 September is simulated by all simulations. However, the timing is different. CONTROL and ASSIM_NORAD

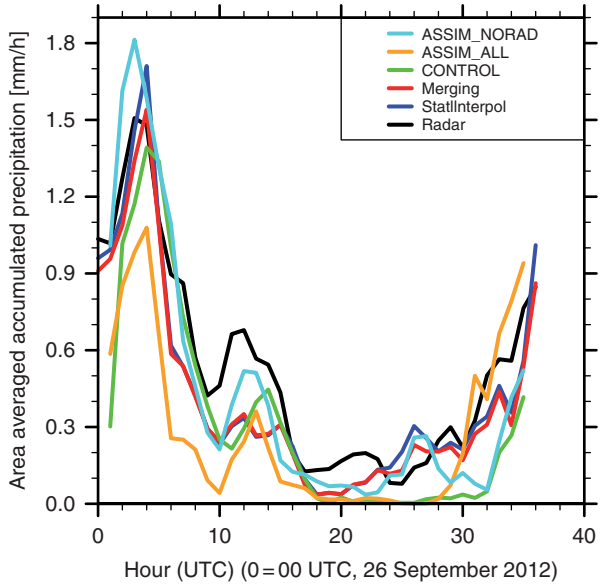

Fig. 12. Time series of hourly accumulated and area averaged precipitation amounts (mm/h) from 00 UTC, 26 September 2012 until 12 UTC, 27 September 2012 for spatially interpolated rain gauge data (blue), precipitation derived from Wideumont radar data (black), a merged product of the two (red) and the three model simulations CONTROL (green), ASSIM_NORAD (cyan) and ASSIM_ALL (orange).

overestimate the intensity, while ASSIM_ALL tends to underestimate it. In the late afternoon of the 26 September and during the night to the 27th, the simulated amounts of precipitation in the CONTROL and ASSIM_ALL simulations were small. The observed intensification of precipitation in the second half of the night is not captured. This is better represented in the ASSIM_NORAD simulation.

During the morning of 27 September, the amount of precipitation increases due to the intensification of convection over the verification domain. This tendency is seen in all three simulations. However, the timing is different. Whereas the observations exhibit a more gradual increase with time starting already during the night, the behaviour is different in the model simulations. In CONTROL and ASSIM_ALL, the intensity of precipitation remains low until the morning of 27 September 2012, followed by a rapid intensification, two hours earlier in ASSIM_ALL. ASSIM_NORAD, on the other hand, follows the gradual increase during the first half of the night and drops in the morning of 27 September before the rapid increase follows along with that of the CONTROL simulation.

This comparison shows how dangerous it is to found the verification only on time series of area averaged precipitation amounts. Many results of the above qualitative comparisons are hidden by the spatial averaging.

4.3. Verification over Germany with REGNIE

The 24-hour accumulated precipitation from 06 UTC, 26 September until 06 UTC, 27 September 2012 of the model simulations was compared with the REGNIE product of DWD. Figure 13 shows the 24-hour accumulated precipitation of REGNIE and the absolute differences MODEL – REGNIE for the three simulations.

The 24-hour accumulated precipitation field shows a band-like structure of precipitation stretching from southwestern to northeastern Germany. In northeastern Germany, the precipitation amounts are clearly smaller due to the stronger frontal activity in central and southern Germany. The western part of Germany shows smaller amounts of precipitation since the front has already passed the area before the accumulation period. The occurrence of convection is seen as patchy or band-like regions of enhanced precipitation over western and northwestern Germany.

As also suggested by the above comparisons with radar, all model simulations underestimate the frontal activity along the rain band over Germany. Furthermore, all simulations overestimate the precipitation in southeastern Germany. The latter can be associated with the strong precipitation simulated by all experiments over the Alps.

The CONTROL simulation shows the strongest underestimation of the frontal precipitation, especially over central and southern Germany. To the rear of the front, a tendency to overestimate the convective activity is seen over northwestern Germany. The underestimation of frontal precipitation is reduced in the ASSIM_NORAD simulation. To the rear of the front, clear overestimation of precipitation in a band-like region from the Saarland in Western Germany northeastwards to the Baltic Sea is seen. This is caused by the more diffusive representation of the front when the assimilation of conventional observations is applied. This was also discussed above during the comparison of reflectivity and hourly accumulated precipitation. The simulation where all data including reflectivity and radial velocity from radar are assimilated (ASSIM_ALL) compares best with REGNIE. The simulated amounts of precipitation in central and southern Germany along the rain band are, as in the other simulations, underestimated. Due to the narrowing of the front with the assimilation of radar, no overestimation to the rear of the front is seen. This dry band between the front and the following showers is best represented in ASSIM_ALL and demonstrates the improvement in the localisation of precipitation due to the assimilation of radar data. Since no radar data were assimilated over Germany, this also demonstrates the beneficial remote influence of the French radar data over Germany. The comparison of the two simulations with

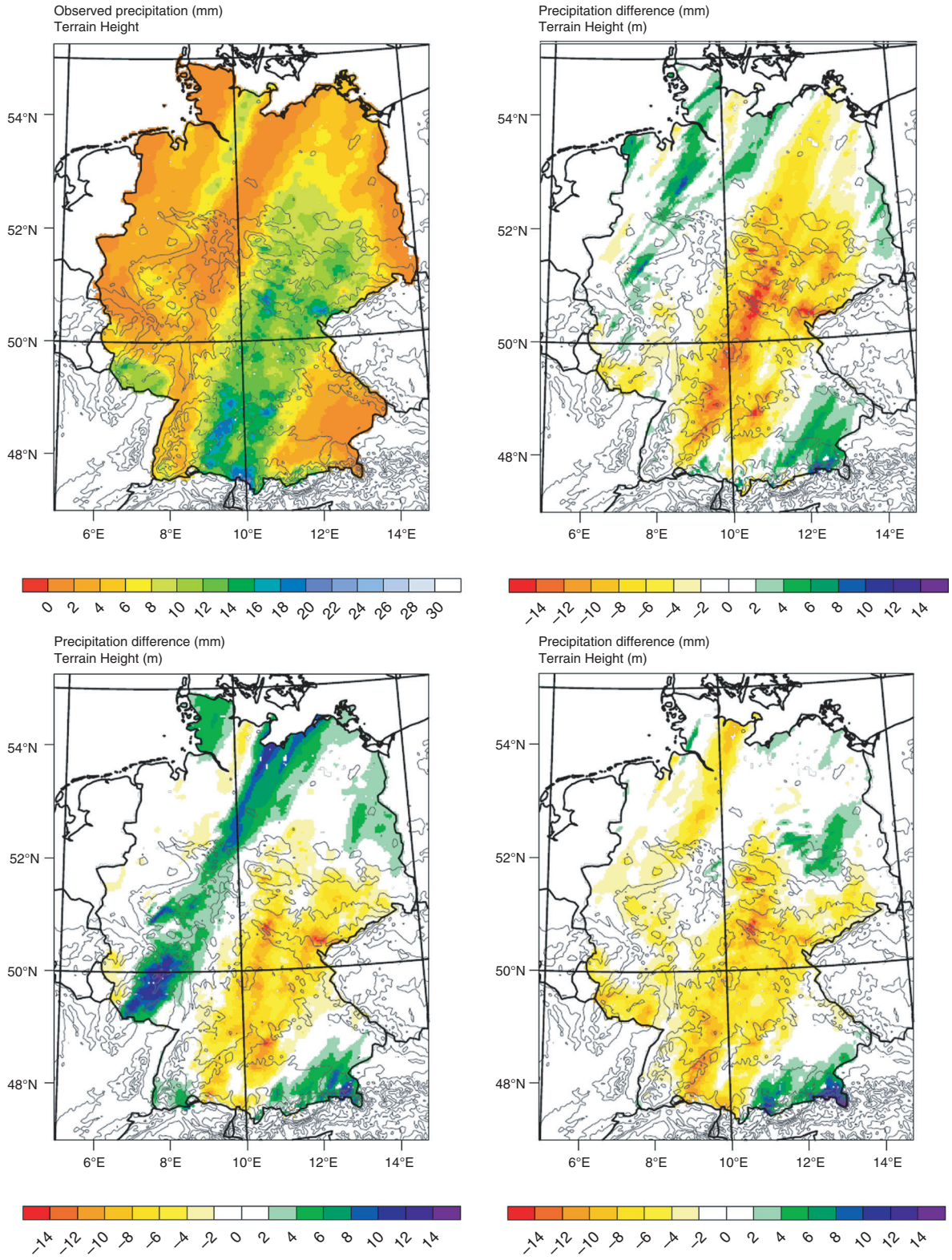

Fig. 13. Comparison of the 24-hourly accumulated precipitation from 06 UTC, 26 September 2012 until 06 UTC, 27 September 2012 of REGNIE (upper left) and MODEL – REGNIE differences of CONTROL (upper right), ASSIM_NORAD (lower left) and ASSIM_ALL (lower right). Contour lines indicate orography.

assimilation demonstrates that the use of radar data is important to correctly capture the location of precipitation.

In addition, verification scores were derived from the comparison with REGNIE. They are summarised in Table 2. Comparing the mean precipitation over Germany, the ASSIM_NORAD simulation provides the best result. The BIAS is as small as −0.28 mm. The CONTROL and ASSIM_ALL simulations show clearly larger BIAS values of −2.18 and −2.19 mm. The large BIAS in ASSIM_ALL may be explained by the simple microphysics scheme in the operator not in balance with the sophisticated microphysics applied in the free forecast. Furthermore, the missing radar guidance over Germany might contribute to the larger BIAS.

Looking to the temporal and spatial distribution of precipitation provides a different picture. The Root Mean Square Error (RMSE) of the CONTROL simulation is 5 mm. This value is reduced by the ASSIM_NORAD simulation to 4.5 mm and by the ASSIM_ALL simulation further to 4.2 mm, indicating the beneficial influence of the assimilation in general and the assimilation of radar data in particular on the representation of the spatial distribution of precipitation. An even better sign for the improvement when radar data is assimilated is the mean correlation of the model simulations to the REGNIE observation. Whereas the CONTROL run shows a low value of 0.2, the ASSIM_NORAD improves this value to 0.29. The assimilation of radar data leads to a further improvement to 0.56. This result is even better if one considers that only radar data over France were assimilated and the scores were derived over Germany. This clearly demonstrates the beneficial influence of the radar data on the representation of the downwind atmosphere. It is to be expected that the result will further improve when the German radar data are also included into the assimilation.

As additional scores, the frequency bias (FB) and the equitable threat score (ETS) were derived. Both scores were calculated for the three precipitation thresholds 1 mm, 5 mm and 10 mm per 24 hours, indicating the performance of the simulation for precipitation events of weak, medium and large intensities. The FB is calculated by dividing the sum of hits and false alarms by the sum of hits and misses. A value larger than 1 means over-prediction and a value lower than 1, under-prediction of the given threshold.

For the weak precipitation events (1 mm/24 hours), the best representation is given by the CONTROL simulation, demonstrating the good performance of the driving ECMWF analysis. ASSIM_NORAD slightly over predicts the weak precipitation events (FB = 1.06), while they are under predicted in the ASSIM_ALL simulation (FB = 0.91). The performance for prediction of medium intensity precipitation events (5 mm/24 h) is reduced for all simulations. The CONTROL and ASSIM_ALL simulations under predict such events (FB = 0.58 for CONTROL and FB = 0.61 for ASSIM_ALL), while the over prediction in ASSIM_NORAD is even stronger (FB = 1.16). The latter is explained by the too broad representation of the front, covering larger areas with larger values of precipitation (see Fig. 13). For the strong precipitation events (10 mm/24 h), the model performance drops to even lower values. Now, all model simulations clearly under predict such events. This is to be expected and is partly caused by the double-penalty problem, punishing forecasts when the precipitation fields are slightly shifted in the forecast and observation. The benefit of data assimilation is nevertheless seen. While the FB for the CONTROL simulation drops to 0.18, ASSIM_NORAD gives a value of 0.38 and ASSIM_ALL of 0.3. The lower value in ASSIM_ALL may be caused by the simple microphysics scheme in the reflectivity forward operator not being in balance with the more sophisticated 2-moment scheme applied in the 1-hour forecasts. Furthermore, the use of only French radar data may contribute to the smaller FB value.

The ETS is calculated by

$$\mathrm{ETS} = \frac{a - a_r}{(a + b + c - a_r)}. \tag{5}$$

Table 2. Verification scores derived from the comparison of the 24-hourly accumulated precipitation (06 UTC, 26 September 2012 until 06 UTC, 27 September 2012) of the model simulations and the DWD REGNIE product

Score		CONTROL	ASSIM_NORAD	ASSIM_ALL
BIAS (mm)		−2.18	−0.28	−2.19
RMSE (mm)		5.02	4.5	4.22
Mean correlation		0.2	0.29	0.56
Equitable threat score	1 mm/24 h	0.1	0.12	0.12
	5 mm/24 h	0.07	0.17	0.29
	10 mm/24 h	0.07	0.06	0.06
Frequency bias	1 mm/24 h	0.99	1.06	0.91
	5 mm/24 h	0.58	1.16	0.61
	10 mm/24 h	0.18	0.38	0.3

Here, a is the number of hits, a_r the number of hits expected by chance, b the number of misses and c the number of false alarms. The number of hits expected by chance a_r is calculated by

$$a_r = \frac{(a+b)(a+c)}{a+b+c+d}, \tag{6}$$

where d is the number of correctly predicted non-events. The denominator in eq. (6) represents the sample size. The ETS has a range from $-1/3$ to 1. Values larger than 0 identify 'skilled' forecasts and a value of 1 represents a perfect forecast, namely that no misses, false alarms and hits expected by chance occur. However, ETS decreases quickly with forecast range and even good forecasts rarely reach values of 0.5. Application of the ETS score can, e.g. be found in Pennelly et al. (2014) or Xue et al. (2013).

For the 1 mm precipitation threshold, the ETS of the CONTROL simulation is 0.1. It rises to 0.12 in ASSIM_NORAD and ASSIM_ALL, indicating that even the weak events are better represented when data assimilation is applied.

Comparing the ETS values for the 5 mm threshold further stresses the advantage of the data assimilation. While the ETS of the CONTROL simulation reduces to 0.07, it increases for ASSIM_NORAD to 0.17 and for ASSIM_ALL further to 0.29. This is a clear indication of the beneficial influence of data assimilation in general, and assimilation of radar data in particular on the prediction of medium-intensity precipitation events. It should be kept in mind that the scores are calculated over Germany where no radar data were assimilated.

As expected, the forecast performance is reduced for the strong precipitation events and it is almost the same for all three simulations. The ETS values are 0.07 for the CONTROL experiment and 0.06 for both the ASSIM_NORAD and the ASSIM_ALL simulations. We would expect a higher ETS value for ASSIM_ALL when radar data over Germany is included in the assimilation.

4.4. Performance of the radar data assimilation and impact to other variables

In the previous subsection, we found a reasonable performance of the CONTROL simulation downscaled from the ECMWF operational analysis. However, the frontal movement is too rapid and the degree of organisation of the convection to the rear of the front is too low. In the ASSIM_NORAD simulation, the inclusion of observations leads to a stronger front. The too rapid movement is reduced, but it is still present and the organisation of convection to the rear of the front is still too weak. ASSIM_ALL further improves the representation of the reflectivity and precipitation fields. The timing of the frontal movement is now correctly simulated and the degree of organisation of the convection to the rear of the front is improved as compared with the radar composite. However, the differences between the simulations are smaller than expected and clear differences between ASSIM_ALL and the observations remain. The next step is therefore to investigate the performance of the assimilation in general and of radar data in particular, to identify possibilities to optimise the system. It is to be expected that the implementation of such changes will significantly increase the benefit of the model system for QPE. Components, whose optimisation enhances the quality of the system, are the assimilation method itself, the background error covariance matrix **B**, the reflectivity operator and especially the Z-q_r relationship and the operator-internal microphysics scheme.

To investigate the reasons for the observed differences to the radar observations, the assimilation process and their influence on the representation of rain water mixing ratio as well as other variables are examined. For the influence of the assimilation, the 1-hour forecast within the RUC is compared with the analysis of the subsequent 3DVAR for two of the above selected snapshots during the development of the synoptic situation. We focus on 02 UTC, 26 September 2012 when the cold front stretched from southwest to northeast over France and on 12 UTC, 27 September 2012, when the post-frontal convection over France was fully developed. Since radar data were only assimilated over France, we restricted the investigation to the domain marked by the blue frame in Fig. 2. Furthermore, we focus the comparison to model level 14, approximately 1300 m above ground, since large changes of the variables related to the hydrological cycle are found there.

We first look at rain water mixing ratio, directly influenced by the assimilation of radar reflectivity. Afterwards, we extend our view to the influence of the assimilation on other variables by performing the same comparisons for cloud water mixing ratio, water vapour mixing ratio and temperature.

Figure 14 compares the rain water mixing ratio. The left column shows the absolute value for the 1-hour free forecast (first guess for the subsequent assimilation) and the right column shows the difference of the new analysis of the 3DVAR and this 1-hour forecast at analysis time for 02 UTC, 26 September 2012 (top row) and 12 UTC, 27 September 2012 (bottom row). The occurring differences are caused by the assimilation process.

For 02 UTC, 26 September 2012, it is seen that the changes of rain water mixing ratio are largest along the northern part of the front. Especially along the upstream convergence line, larger amounts of rain water are added by the assimilation. Shifts in the precipitation centres are responsible for local differences. Outside the frontal region, the changes are small.

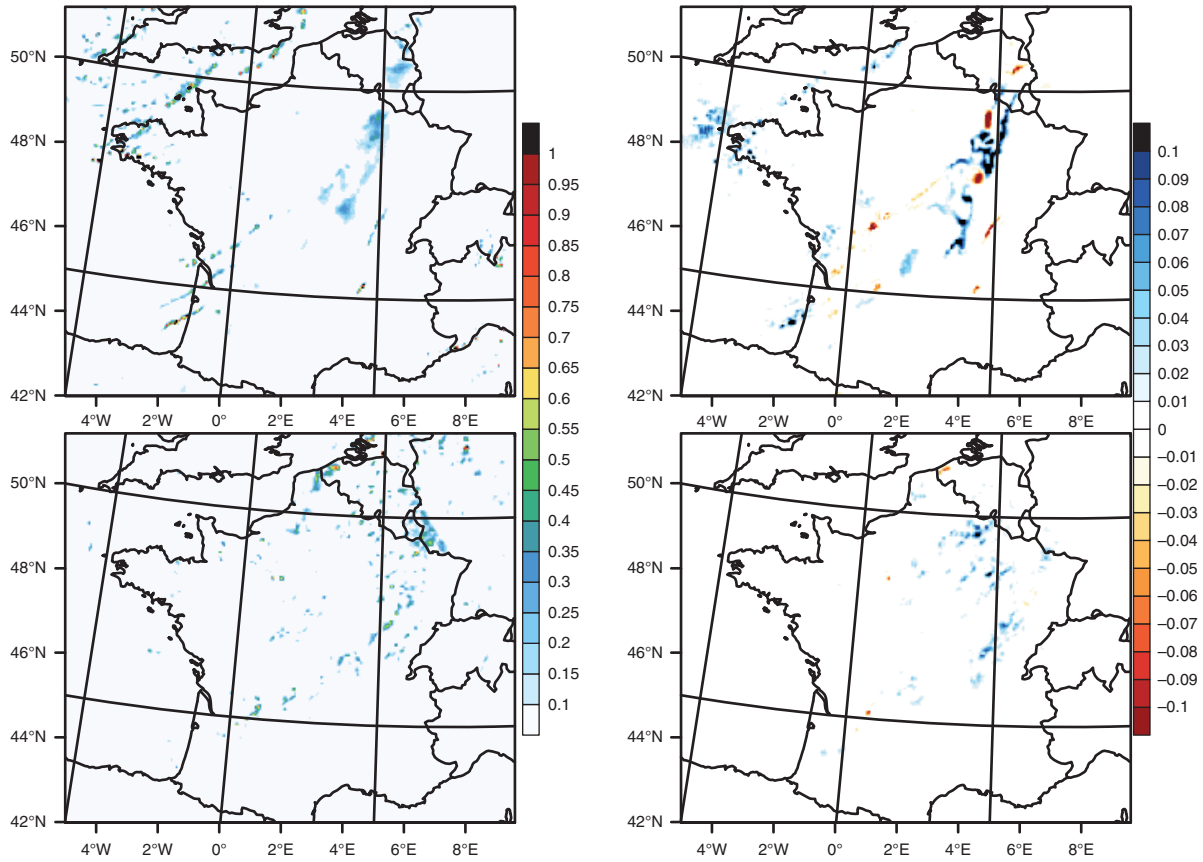

Fig. 14. Comparison of rain water mixing ratio (g/kg) of the 1-hour forecast (First Guess) (left column) and the Analysis – First Guess difference (right column) for 02 UTC, 26 September 2012 (upper line) and 12 UTC, 27 September 2012 (lower line) at model level 14 (approximately 1300 m above ground level).

Along the sharp southern part of the front slight changes are seen caused by shifts of the precipitation cores. Directly to the rear and upstream of the front negative values occur, indicating that the convection is suppressed by the assimilation. Referring to the conceptual model of cyclogenesis in Europe (Browning, 1986; Browning and Roberts, 1994; Browning and Golding, 1995), a cold front is followed by a region where cold air subsides, the so-called post-frontal subsidence zone. A strengthening of the subsidence by the assimilation would explain the reduction of convection. On the other hand, further to the west, the rain water mixing ratio is systematically increased by the assimilation. This tendency is also seen at 12 UTC, 27 September 2012. Now the post-frontal convection is fully evolved over large parts of France and the assimilation of radar data systematically adds rain water especially in the strongest precipitation cores. Figure 15 does the same comparison for cloud liquid water. Since cloud water and rainwater are connected in the cloud microphysics scheme, the same signals compared with the rain water mixing ratio are seen. Cloud water is increased along the front and decreased to the rear and upstream of the front.

Figure 16 compares the water vapour mixing ratio fields in the same way as for the rain water mixing ratio. It is striking that the changes in the water vapour field are of large-scale nature as compared to the differences in rain water mixing ratio. On the one hand, water vapour is part of the conventional observations distributed in the whole model domain. On the other hand, water vapour is implemented in the background error covariance matrix **B** as pseudo relative humidity, responsible for the spatial spreading of the information of the observations in the model domain. At 02 UTC, 26 September 2012, the differences in the region of the front are small. To the rear and upwind parts of the front, especially over central and southern France, water vapour is reduced by the assimilation. This decrease in humidity is in line with the decrease of rain water mixing ratio in the region of the post-frontal subsidence.

At 12 UTC, 27 September 2012, water vapour is increased in the region of most intense convective activity in north-eastern France. The superimposed small-scale influence of convection is seen. Comparing the changes in the water

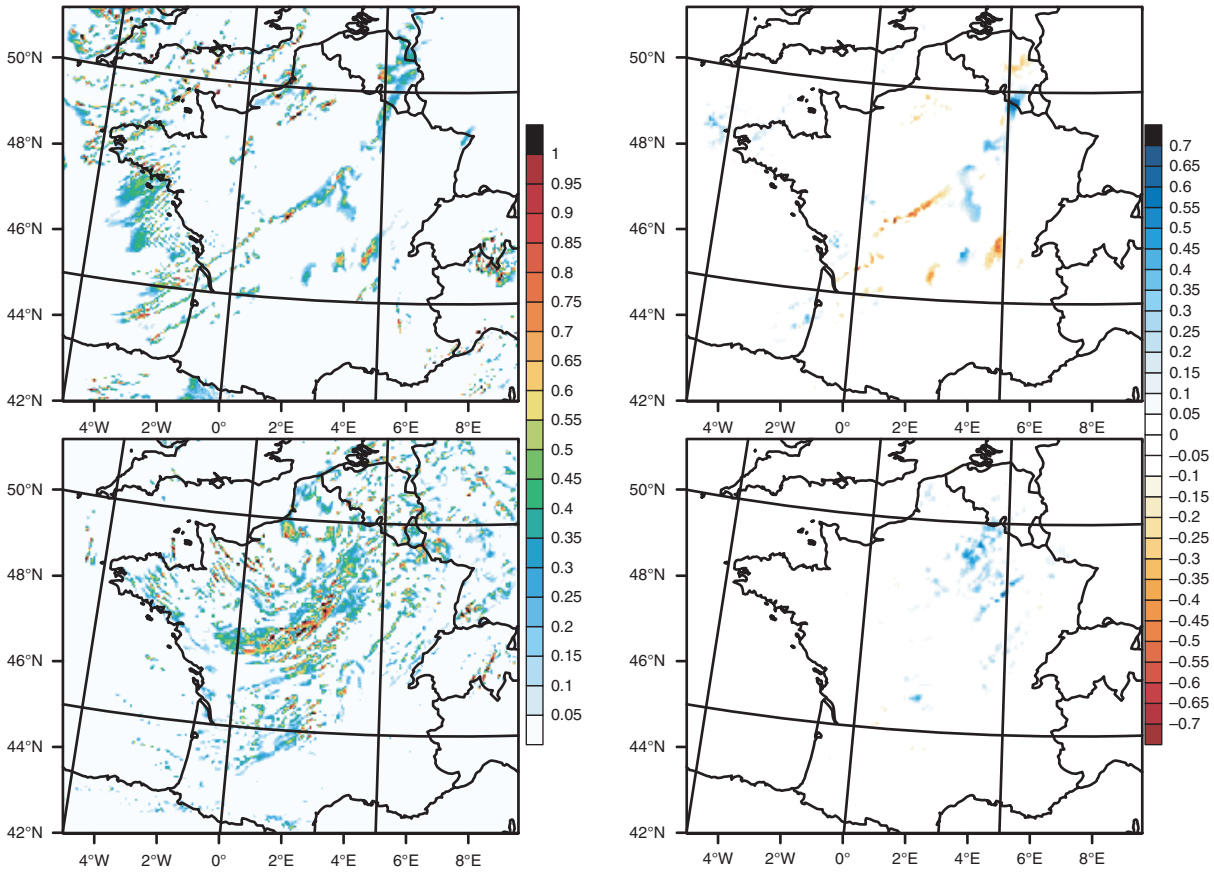

Fig. 15. Same as Fig. 14, but for cloud water mixing ratio (g/kg).

vapour and reflectivity fields, the interplay between the reflectivity forward operator and the cloud microphysics scheme is obvious. Whenever the rainwater mixing ratio is reduced by the assimilation, also the water vapour mixing ratio is reduced and vice versa.

Figure 17 shows the same comparison for temperature. At 02 UTC, 26 September 2012, again large-scale and small-scale changes are seen. The assimilation reduces the temperature on the rear side of the front, especially in the Bay of Biscay. The large-scale changes cover a larger area than the changes in the water vapour field. It is noticeable that, compared to the water vapour field, the small-scale changes in the temperature field are stronger pronounced. This can be explained by the release of latent heat in convective cells. Where convection occurs and water vapour condenses, the cooling is either reduced or even a warming occurs locally. Conversely, lower temperatures occur where evaporation takes place.

At 12 UTC, 27 September 2012, the overall changes in the temperature field are smaller than on the day before. Nevertheless, the release of latent heat in the region of intense convection in northeastern France is noticeable.

5. Summary and conclusions

This study investigated the performance of model-based QPE with WRF and its 3DVAR data assimilation system for a complex case study. In both assimilation experiments, the model was operated in a RUC with a 1-hour frequency. ASSIM_NORAD assimilated all available observations apart from radar data and in ASSIM_ALL, volume data of reflectivity and radial velocity from the French radar network are assimilated in addition. The reference for an assessment of the QPE performance is a 36-hour free forecast downscaled from the ECMWF operational analysis (CONTROL).

Qualitative comparisons with radar reflectivity composite products showed that the frontal development is reasonably represented by the CONTROL simulation. However, the front moved more rapidly than observed and showed a more diffuse structure with lower intensity as compared to the radar reflectivity composite. The development of convection to the rear of the front started too late and its organisation into band-like structures was not simulated. ASSIM_NORAD reduced the movement speed and the convection

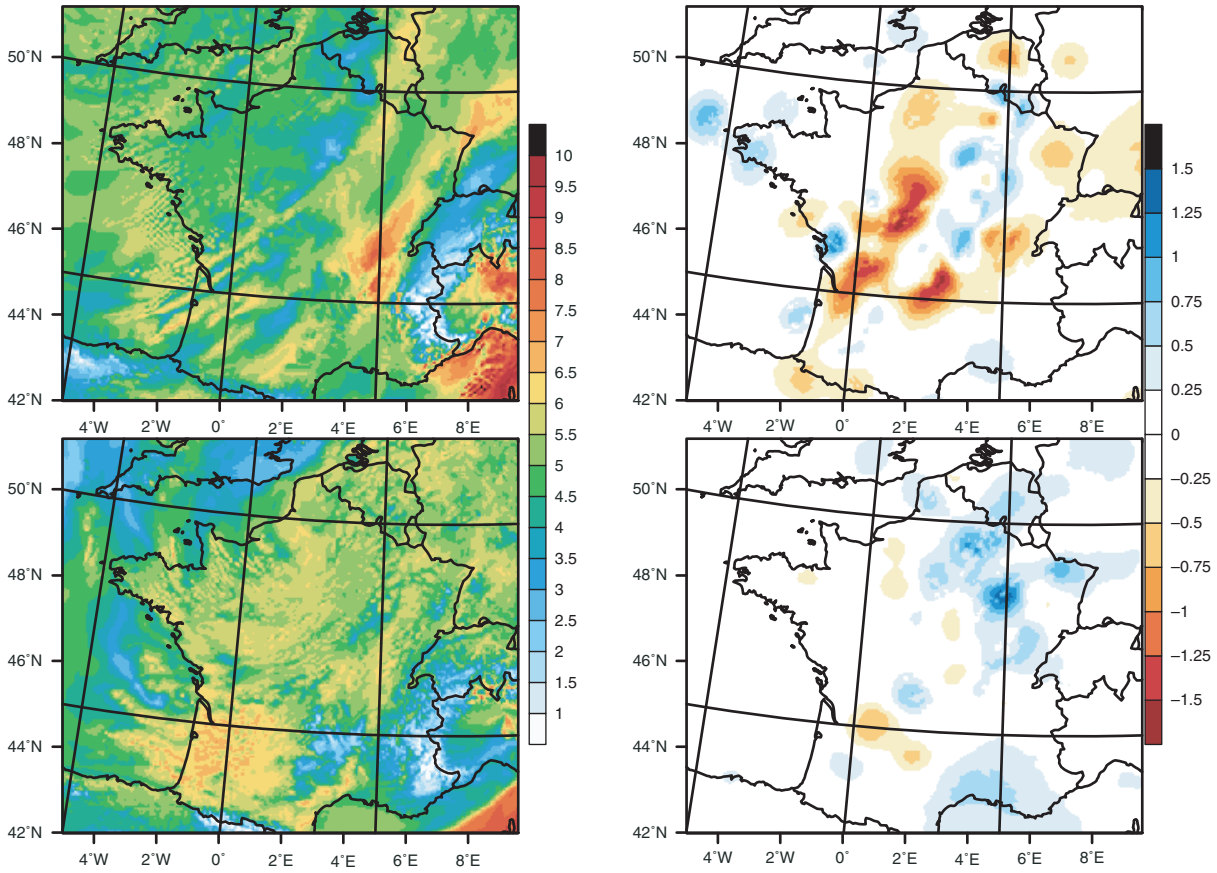

Fig. 16. Same as Fig. 14, but for water vapour mixing ratio (g/kg).

that developed to the rear of the front was intensified. However, the front still moved too rapidly and the convection was still less organised as compared to the radar composite. Both the timing of the front and the organisation of convection behind the cold front were further improved in the ASSIM_ALL simulation. The frontal system was sharpened and even the location of single convective elements and band-like reflectivity structures, seen in the observations, were reproduced. This demonstrates the necessity to assimilate volume radar data to reproduce mesoscale convective structures. We expect that this becomes more important as the model resolution increases.

The representation of frontal precipitation was systematically underestimated by the model simulations, although the situation improved when the assimilation of observations, and here especially the assimilation of radar data, was included. The opposite holds for precipitation in the region of the developing convection to the rear of the front. Here, the model overestimated the intensity and size of the convective cells. Possible causes are the model resolution, the selected cloud microphysics scheme, or the reflectivity forward operator. Nevertheless, comparison of the 24-hourly accumulated precipitation sum of the model simulations with the REGNIE product of DWD and the derivation of forecast scores confirmed that the assimilation of radar data is necessary for a best possible representation of the spatial and temporal distribution of precipitation. The comparison of time series of hourly accumulated precipitation in a small verification domain centred over Luxembourg revealed in addition that it is necessary to always include different approaches when forecasts have to be verified. The timing error of the CONTROL simulation and the spatial and temporal improvements of ASSIM_ALL were hidden by the calculation of time series of spatially averaged precipitation sums.

From the above results, we conclude that radar data with good coverage and quality is the most important observation to improve the temporal and spatial simulation of precipitation. The way in which the data is included is, however, very important for the performance. The 3DVAR system applies a background error covariance matrix **B** that is derived from a monthly set of forecast differences. The so-called 'error of the day', namely the flow dependence of the background error is not included into the assimilation, leading to spatial

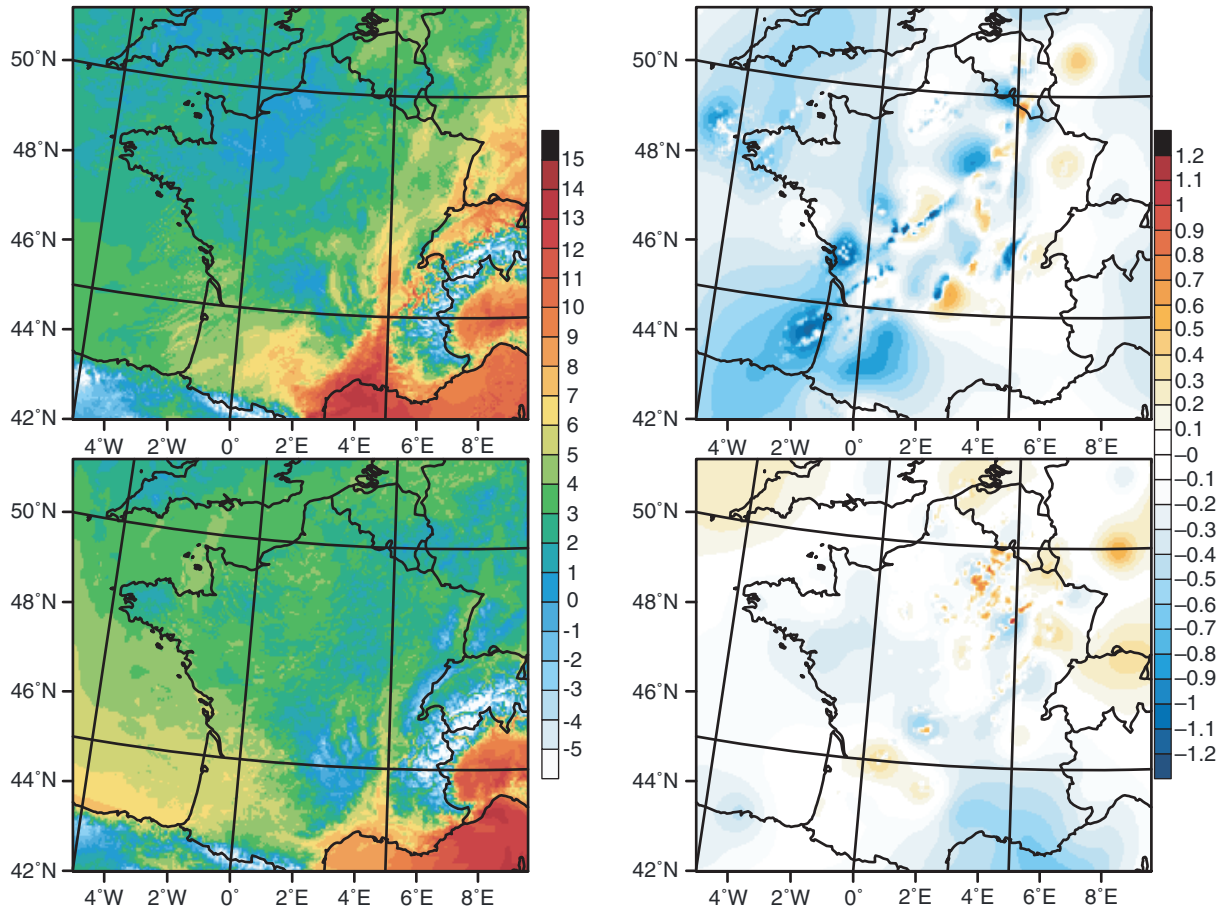

Fig. 17. Same as Fig. 14, but for temperature (°C).

and temporal inaccuracies during the transport of the observed signal into the analysis.

Other critical parts of the assimilation system are the forward operators. Although the parameter translation for the radial velocity is relatively straightforward, the Z-q_r relationship, necessary to calculate the observed reflectivity Z, is critical. It depends on the synoptic situation and the region, and hence the derivation of a single all-purpose relationship is not possible (Jameson and Kostinski, 2001). Currently, the Z-q_r relation of Sun and Crook (1997) is applied in the WRFDA. A potential improvement could be to optimise this relation for different regions and synoptic situations with observations (e.g. from the disdrometers and/or micro rain radars (MRRs) operated during the CAOS project). It has already been shown that improved Z-R relations lead to an improved representation of precipitation (e.g. Picciotti et al., 2010; Neuper and Ehret, 2014). This might also lead to a better balance between the different microphysics schemes applied in the reflectivity forward operator and the free forecast. The quality control of the 3DVAR only accepts observations when the difference (observation-minus-background) is less than 15 dB. This can be especially problematic in convective situations where the developing cells are located differently in the observation and the model background or no convection is present in either the model background or the observation.

Another weakness of the currently applied reflectivity operator is that it does not handle frozen hydrometeors. Therefore, observations above 3500 m height were discarded for the assimilation. This might have a detrimental influence on the vertical evolution of cloud systems, and the balancing of the cloud microphysics might be problematic when only a part of the atmospheric column is changed by the operator. This exclusion of the ice phase in the calculation of the reflectivity, and the setting of a threshold height might lead to an overestimation of Z in regions where cells reach the threshold height, since the backscattered signal of liquid hydrometeors are stronger than that of graupel and snow. Volume radar data revealed that the threshold for our experiments was set too high – the observed height of the bright band was at 2300 m instead of 3500 m, explaining at least part of the overestimation of convection. In addition, ice particles are often mixed downward into the lower troposphere due to

convective mixing, which is also not captured by the current version of the operator.

The general moistening by the assimilation within regions of developing convection suggests that the model tends to dry the atmosphere during the 1-hour forecast. This might be caused by imbalances introduced by the assimilation and the following model spin-up, counteracting the changes included by the assimilation. This spin-up is influenced by the cycling frequency of the RUC. The application of a digital filter – designed to reduce small-scale noise implemented into the initialisation may also help to reduce the imbalances. However, the filter might also destroy small-scale features important for high-resolution QPE. The influence of the RUC frequency and the digital filter will be tested with sensitivity studies in the future.

With these considerations in mind, several improvements of the system are conceivable:

- Optimisation of the assimilation system (assimilation method, background error covariance matrix, RUC cycle, digital filter)
- Optimisation of the forward operator in the assimilation system (Z-q_r relation, inclusion of the ice phase into the operator microphysics, threshold of reflectivity error)
- Inclusion of further observations, such as high-resolution volume data of water vapour and temperature, to improve the 3D structure of the atmosphere before development of clouds and precipitation is initiated. Such observations are available from Lidar developed and operated by the Institute of Physics and Meteorology for several field campaigns (e.g. Radlach et al., 2008; Behrendt et al., 2009, 2011)
- Assimilation of data from polarisation radar to better adjust the cloud microphysics to observations. Within the CAOS project, a corresponding forward operator for the WRF model is currently being developed.
- Wattrelot et al. (2014) described a methodology to avoid the strong nonlinearity and dependence on the reflectivity forward operator. With the aid of reflectivity error statistics, they derived profiles of relative humidity and continued the assimilation of them.

This study is a promising first step towards a more intense use of numerical models for QPE. Nevertheless, the current system has drawbacks and can therefore not yet compete with observation-based QPE methods. With an optimised system available after detailed sensitivity studies, downscaling to higher resolutions and more detailed comparisons with observation-based QPE are the next steps.

6. Acknowledgements

The German Research Foundation (DFG) is acknowledged for funding the Collaborative research group 'Catchments As Organized Systems' (CAOS) (FOR 1598), in which this investigation is embedded. The MSG satellite composites were provided from the NERC satellite receiving station of the Dundee University, Scotland from the website http://www.sat.dundee.ac.uk/. The RADOLAN radar products were provided by the data service of the German Meteorological Service (DWD). ECMWF is acknowledged for providing the operational analysis data. The data were converted to NetCDF with the WRADLIB package (http://wradlib.bitbucket.org/).

The WRF developer team and the contributing community are thanked for their tireless efforts to improve the model system. The simulations were performed at the High Performance Computing Center (HLRS) in Stuttgart.

Finally, the four anonymous reviewers are thanked for their detailed comments. They contributed to the improvement of the manuscript.

References

Ablash, S., Sahai, A. K., Mohankumar, K., George, J. P. and Das, S. 2012. Assimilation of Doppler radar radial velocity and reflectivity observations in WRF 3DVAR system for short-range forecasting of convective storms. *Pure Appl. Geophys.* **169**, 2047–2070.

Barker, D. M., Huang, W., Guo, Y.-R. and Xiao, Q. N. 2004. A three-dimensional variational (3DVAR) data assimilation system for MM5. Implementation and initial results. *Mon. Weather Rev.* **132**, 897–914.

Barker, D. M., Huang, X.-Y., Lui, Z., Augliné, T., Zhang, Z. and co-authors. 2012. The weather research and forecasting model's variational/ensemble data assimilation system WRFDA. *Bull. Am. Meteorol. Soc.* **93**(6), 831–843.

Bartels, H. 2004. RADOLAN. Routineverfahren zur Online-Aneichung der Radarniederschlagsdaten mit Hilfe von automatischen Bodenniederschlagsstationen (Ombrometer). *Schlussbericht*. Deutscher Wetterdienst.

Bartels, H., Weigel, E., Klink, E., Kohler, S., Reich, T. and co-authors. 2005. *Projekt RADVOR-OP Radargestützte, zeitnahe Niederschlagsvorhersage für den operationellen Einsatz (Niederschlag-Nowcasting-System)*. Technical Report, Deutscher Wetterdienst, 123 p.

Bauer, H.-S., Weusthoff, T., Dorninger, M., Wulfmeyer, V., Schwitalla, T. and co-authors. 2011. Predictive skill of a subset of the D-PHASE multi-model ensemble in the COPS region. COPS Special Issue. *Q. J. Roy. Meteorol. Soc.* **137**, 287–305. DOI: 10.1002/qj.715.

Behrendt, A., Pal, S., Aoshima, F., Bender, M., Blyth, A. and co-authors. 2011. Observation of convection initiation processes with a suite of state-of-the-art research instruments during COPS IOP8b. *Q. J. Roy. Meteorol. Soc.* **137**, 81–100. DOI: 10.1002/qj.758.

Behrendt, A., Wulfmeyer, V., Riede, A., Wagner, G., Pal, S. and co-authors. 2009. 3-Dimensional observations of atmospheric

humidity with a scanning differential absorption Lidar. In: *Remote Sensing of Clouds and the Atmosphere XIV* (eds. R. H. Picard, K. Schäfer, A. Comeron and co-editors.), SPIE Conference Proceeding Vol. 7475, ISBN: 9780819477804, 2009, Art. No. 74750L, International Society for Optics and Photonics (SPIE), Bellingham, WA, USA. DOI: 10.1117/12.835143.

Berenguer, M. and Zawadzki, I. 2008. A study of the error covariance matrix of radar rainfall estimates in stratiform rain. *Weather Forecast*. **23**, 1085–1101. DOI: 10.1175/2008waf2222134.1.

Berne, A., Ten Heggeler, M., Uijlenhoet, R., Delobbe, L., Dierickx, P. and co-authors. 2005. A preliminary investigation of radar rainfall estimation in the Ardennes region and a first hydrological application for the Ourthe catchment. *Nat Hazards Earth Syst Sci*. **5**, 267–274.

Brandes, E. A., Zhang, G. and Vivekanandan, J. 2004a. Comparison of polarimetric radar drop size distribution retrieval algorithms. *J. Atmos. Ocean. Technol*. **21**, 584–598.

Brandes, E. A., Zhang, G. and Vivekanandan, J. 2004b. Drop size distribution retrieval with polarimetric radar: model and application. *J. Appl. Meteorol*. **43**, 461–475.

Browning, K. A. 1986. Conceptual models of precipitation systems. *Weather Forecast*. **1**, 23–41.

Browning, K. A. and Golding, B. W. 1995. Mesoscale aspects of a dry intrusion within a vigorous cyclone. *Q. J. R. Meteorol. Soc*. **121**, 463–493.

Browning, K. A. and Roberts, N. M. 1994. Structure of a frontal cyclone. *Q. J. Roy. Meteorol. Soc*. **120**, 1535–1557.

Cao, Q., Zhang, G., Brandes, E., Schuur, T., Ryzhkov A. and co-authors. 2008. Analysis of video disdrometer and polarimetric radar data to characterize rain microphysics in Oklahoma. *J. Appl. Meteorol. Clim*. **47**, 2238–2255.

Dorninger, M., Schneider, S. and Steinacker, R. 2008. On the interpolation of precipitation data over complex terrain. *Meteorol. Atmos. Phys*. **101**, 175–189.

Dotzek, N. and Beheng, K.-D. 2001. The influence on deep convective motions on the variability of Z-R relations. *Atmos. Res*. **59**, 15–39.

Dudhia, J. 1989. Numerical study of convection observed during winter monsoon experiment using a mesoscale two-dimensional model. *J. Atmos. Sci*. **46**, 3077–3107.

Germann, U., Berenguer, M., Sempere-Torres, D. and Zappa, M. 2009. REAL – Ensemble radar precipitation estimation for hydrology in a mountainous region. *Q. J. Roy. Meteorol. Soc*. **135**, 445–456. DOI: 10.1002/qj.375.

Goudenhoofdt, E. and Delobbe, L. 2009. Evaluation of radar-gauge merging methods for quantitative precipitation estimates. *Hydrol. Earth Syst. Sci*. **13**, 195–203.

Hamill, T. M. 2014. Performance of operational precipitation forecast guidance during the 2013 Colorado Front-Range floods. *Mon. Weather Rev*. **142**, 2609–2618. DOI: 10.1175/MWR-D-14-00007.1.

Hong, S.-Y., Noh, Y. and Dudhia, J. 2006. A new vertical diffusion package with an explicit treatment of entrainment processes. *Mon. Weather Rev*. **134**, 2318–2341.

Hong, S.-Y., Park, H., Cheong, H.-B., Esther Kim, J.-E., Koo, M.-S. and co-authors. 2013. The global/regional integrated model system (GRIMs). *Asia-Pacific J. Atmos. Sci*. **49**, 219–243. DOI: 10.1007/s13143-013-0023-0.

Huang, X.-Y., Gao, F., Jacobs, N. and Wang, H. 2013. Assimilation of wind speed and wind direction observations. A new formulation and results from idealized experiments. *Tellus A*. **65**, 19936.

Iacono, M. J., Delamere, J. S., Mlawer, E. J., Shephard, M. W., Clough, S. A. and co-authors. 2008: Radiative forcing by long-lived greenhouse gases: calculations with the AER radiative transfer models. *J. Geophys. Res*. **113**, D13103. DOI: 10.1029/2008JD009944.

Ide, K., Courtier, P., Ghil, M. and Lorenc, A. C. 1997. Unified notation for data assimilation: operational, sequential and variational. *J. Meteorol. Soc. Jpn*. **75**, 181–189.

Jameson, A. R. and Kostinski, A. B. 2001. What is a raindrop size distribution? *Bull. Am. Meteorol. Soc*. **82**, 1169–1177.

Kober, K., Craig, G., Keil, C. and Dörnbrack, A. 2010. Blending a probabilistic nowcasting method with a high-resolution ensemble for convective precipitation forecasts. *Q. J. Roy. Meteorol. Soc*. **138**, 755–768. DOI: 10.1002/qj.939.

Lean, H. W., Clark, P. A., Dixon, M., Roberts, N. H., Fitch, A. and co-authors. 2008. Characteristics of high-resolution versions of the Met Office Unified model for forecasting convection over the United Kingdom. *Mon. Weather Rev*. **136**, 3408–3424.

Lee, G., Seed, A. W. and Zawadzki, I. 2007. Modeling the variability of drop size distributions in space and time. *J. Appl. Meteorol. Clim*. **46**, 742–756. DOI: 10.1175/jam2505.1.

Lee, G. and Zawadzki, I. 2005. Variability of drop size distributions: time-scale dependence of the variability and its effects on rain estimation. *J. Appl. Meteorol*. **44**, 241–255.

Liu, J., Bray, M. and Han, D. 2013a. A study on WRF radar data assimilation for hydrological rainfall prediction. *Hydrol. Earth Syst. Sci*. **17**, 3095–3110.

Liu, J., Bray, M. and Han, D. 2013b. Exploring the effect of data assimilation by WRF-3DVAR for numerical rainfall prediction with different types of storm events. *Hydrol. Proc*. **27**, 3627–3640.

Lopez, P. 2013. Experimental 4D-Var assimilation of SYNOP rain gauge data at ECMWF. *Mon. Weather Rev*. **141**(5), 1527–1544.

Milovac, J., Ingwersen, J. and Warrach-Sagi, K. 2014a. Soil texture forcing data for the whole world for the Weather Research and Forecasting (WRF) Model of the University of Hohenheim (UHOH) based on the Harmonized World Soil Database (HWSD) at 30 arc-second horizontal resolution. *World Data Center Clim*. DOI: 10.1594/WDCC/WRF_NOAH_HWSD_world_TOP_SOILTYP.

Milovac, J., Ingwersen, J. and Warrach-Sagi, K. 2014b. Top soil texture forcing data for the area of Germany for the Weather Research and Forecasting (WRF) Model based on the Bodenubersichtskarte (BUK) at a scale 1:1000000 (BUK1000) and provided by the University of Hohenheim (UHOH). *World Data Center for Clim*. DOI: 10.1594/WDCC/WRF_NOAH_BUK_Ger_top_SOILTYP.

Montmerle, T. and Faccani, C. 2009. Mesoscale assimilation of radial velocities from Doppler radars in a preoperational framework. *Mon. Weather Rev*. **137**, 1939–1953.

Moreau, E., Testud, J. and Le Bouar, E. 2009. Rainfall spatial variability observed by X-band weather radar and its implication for the accuracy of rainfall estimates. *Adv. Water Resour*. **32**, 1011–1019. DOI: 10.1016/j.advwatres.2008.11.007.

Morrison, H., Thompson, G. and Tatarskii, V. 2009. Impact of cloud microphysics on the development of trailing stratiform precipitation in a simulated squall line: comparison of one- and two-moment schemes. *Mon. Weather Rev.* **137**, 991–1007.

Neuper, M. and Ehret, U. 2014. Comparison of measured drop size distribution and retrieved Z/R relations with the distribution of reflectivity patterns in the 3D-radar image. In: *Proceeding of the ERAD 2014, Garmisch-Partenkirchen (Germany) – 8th European Radar Conference ERAD 2014*, Garmisch-Partenkirchen, Germany, 1–5 September 2014.

Niu, S. J., Jia, X. C., Sang, J. R., Liu, X. L., Lu, C. S. and co-authors. 2010. Distributions of raindrop sizes and fall velocities in a semiarid plateau climate: convective versus stratiform rains. *J. Appl. Meteorol. Clim.* **49**, 632–645. DOI: 10.1175/2009jamc2208.1.

Niu, G.-Y., Yang, Z.-L., Mitchell, K. E., Chen, F., Ek, M. B. and co-authors. 2011. The community Noah land surface model with multiparameterization (Noah-MP): model description and evaluation with local-scale measurements. *J. Geophys. Res.* **116**, D12109. DOI: 10.1029/2010JD015139.

Nurmi, P. 2003. Recommendations on the verification of local weather forecasts. *ECMWF technical memorandum*, European Center for Medium Range Weather Forecasting, Shinfield Park, Reading, **430**, 19 pp.

Parrish, D. F. and Derber, J. C. 1992. The National Meteorological Centre's spectral statistical-interpolation analysis system. *Mon. Weather Rev.* **120**, 1747–1763.

Pennelly, C., Reuter, G. and Flesch, T. 2014. Verification of the WRF model for simulating heavy precipitation in Alberta. *Atmos. Res.* **135–136**, 172–192.

Peters, G., Fischer, B., Munster, H., Clemens, M. and Wagner, A. 2005. Profiles of raindrop size distributions as retrieved by microrain radars. *J. Appl. Meteorol.* **44**, 1930–1949.

Picciotti, E., Montopoli, M., Mori, S. and Marzano, F. S. 2010. Statistical calibration of surface rain fields derived from C-band Mt. Midia operational radar in central Italy. In: *Proceeding of the 10th European Conference on Radar in Meteorology (ERAD2010)*, Sibiu, Romania.

Radlach, M., Behrendt, A. and Wulfmeyer, V. 2008. Scanning rotational Raman Lidar at 355 nm for the measurement of tropospheric temperature fields. *Atmos. Chem. Phys.* **8**, 159–169.

Rossa, A., Bruen, M., Frühwald, D., Macpherson, B., Holleman, I. and co-authors. 2005. *COST 717 Use of Radar Observations in Hydrological and NWP Models* Vol. 292. European Co-Operation in the Field of Scientific and Technical Research. COST Office, Belgium.

Rossa, A., Del Guerra, F. and Leuenberger, D. 2009. An empirical radar data quality function. In: *Proceeding of the AMS Radar Conference*, Williamsburg, VA, 5–9 October 2009.

Rotach, M. W., Ambrosetti, P., Ament, F., Appenzeller, C., Arpagaus, M. and co-authors. 2009. MAP D-PHASE: real-time demonstration of weather forecast quality in the Alpine region. *Bull. Am. Meteorol. Soc.* **90**, 1321–1336. DOI: 10.1175/2009 BAMS2776.1.

Saito, K., Ishida, J., Aranami, K., Hara, T., Segawa, T. and co-authors. 2007. Nonhydrostatic atmospheric models, and operational development at JMA. *J. Meteorol. Soc. Jpn.* **85B**, 271–304.

Sauvageot, H. 1992. *Radar Meteorology*. Artech House Publishing, Norwood, MA, USA, 384 pp.

Schwartz, C. S. 2014. Reproducing the September 2013 record-breaking rainfall over the Colorado front range with high-resolution WRF forecasts. *Weather Forecast.* **29**, 393–402.

Schwitalla, T., Bauer, H.-S., Wulfmeyer, V. and Aoshima, F. 2011. High-resolution simulation over central Europe: assimilation experiments with WRF 3DVAR during COPS IOP9c. *Q. J. Roy. Meteorol. Soc.* **137**, 156–175. DOI: 10.1002/qj.721.

Schwitalla, T., Zängl, G., Bauer, H.-S. and Wulfmeyer, V. 2008. Systematic errors of QPF in low-mountain regions. Special Issue on Quantitative Precipitation Forecasting. *Meteorol. Zeitschrift.* **17**, 903–919. DOI: 10.1127/0941-2948/2008/0338.

Schwitalla, T. and Wulfmeyer, V. 2014. Radar data assimilation experiments using the IPM WRF rapid update cycle. *Meteorol. Zeitschrift.* **23**, 79–102. DOI: 10.1127/0941-2948/2014/0513.

Seity, Y., Brousseau, P., Malardel, S., Hello, G., Bénard, P. and co-authors. 2011: The AROME-France Convective-Scale Operational Model. *Mon. Weather Rev.* **139**, 976–991. DOI: 10.1175/2010MWR3425.1.

Shepard, D. 1968. A two-dimensional interpolation function for irregularly-spaced data. *Proc. 1968 ACM Natl. Conf.* 517–524. DOI: 10.1145/800186.810616.

Skamarock, W. C., Klemp, J. B., Dudhia, J., Gill, D. O., Barker, D. M. and co-authors. 2008. *A Description of the Advanced Research WRF Version 3*. NCAR Tech. Note TN-475+STR, 113 pp.

Smith, E. A., Asrar, G., Yoji, F., Gianti, A., Mugnai, A. and co-authors. 2007. The international global precipitation measurement (GPM) program and mission: an overview. In: *Measuring Precipitation from Space: URAINSAT and the Future* (eds. V. Levizzani and F. J. Turk), Springer, pp. 611–653.

Steinacker, R., Ratheiser, M., Bica, B., Chimani, B., Dornimnger, M. and co-authors. 2006. A mesoscale data analysis and downscaling method over complex terrain. *Mon. Weather Rev.* **134**, 2758–2771.

Steppeler, J., Doms, G., Schaettler, U., Bitzer, H. W., Gassmann, A. and co-authors. 2003. Meso-gamma scale forecasts using the non-hydrostatic model LM. *Meteorol. Atmos. Phys.* **82**, 257–268.

Sugimoto, S., Crook, N. A., Sun, J., Xiao, Q. and Barker, D. M. 2009. An examination of WRF 3DVAR data assimilation and its capability in retrieving unobserved variables and forecasting precipitation through observing system simulation experiments. *Mon. Weather Rev.* **137**, 4011–4029.

Sun, J. and Crook, N. A. 1997. Dynamical and microphysical retrieval from Doppler radar observations using a cloud model and its adjoint. Part I: Model development and simulated data experiments. *J. Atmos. Sci.* **54**, 1624–1661.

Tabary, P., Guibert, F., Perier, L. and Parent-du Charlet, J. 2006. An operational triple-PRT Doppler scheme for the French radar network. *J. Atmos. Ocean. Technol.* **23**, 1645–1656.

Tafferner, A., Forster, C., Hagen, M., Keil, C., Zinner, T. and co-authors. 2008. Development and propagation of severe thunderstorms in the upper Danube catchment area: towards an integrated nowcasting and forecasting system using real-time data and high-resolution simulations. *Meteorol. Atmos. Phys.* **101**, 211–227.

Tahanout, M., Parent Du Chatelet, C. and Augros, C. 2009. New multiple-PRT scheme for Météo-France Doppler radar network to improve spectral moment estimation of weather radar signal and ground clutter filtering. In: *34th AMS Conference on Radar Meteorology*, American Meteorological Society, USA.

Tapiador, F. J., Checa, R. and De Castro, M. 2010. An experiment to measure the spatial variability of rain drop size distribution using sixteen laser disdrometers. *Geophys. Res. Lett.* **37**(6), L16803. DOI: 10.1029/2010gl044120.

Thiessen, A. H. 1911. Precipitation averages for large areas. *Mon. Weather Rev.* **39**, 1082–1089.

Troemel, S., Simmer, C., Braun, J., Gerstner, T. and Griebel, M. 2009. Toward the use of integral radar volume descriptors for quantitative areal precipitation estimation: results from Pseudo radar observations. *J. Atmos. Ocean. Technol.* **26**, 1798–1813. DOI: 10.1175/2009jtecha1203.1.

Villarini, G. and Krajewski, W. F. 2010. Review of the different sources of uncertainty in single polarization radar-based estimates of rainfall. *Surv. Geophys.* **31**, 107–129. DOI: 10.1007/s10712-009-9079-x.

Wattrelot, E., Caumont, O. and Mahfouf, J.-F. 2014. Operational implementation of the 1D+3D-Var assimilation method of radar reflectivity data in the AROME model. *Mon. Weather Rev.* **142**, 1852–1873.

Weusthoff, T., Ament, F., Arpagaus, M. and Rotach, M. W. 2010. Assessing the benefits of convection-permitting models by neighborhood verification: examples from MAP D-PHASE. *Mon. Weather Rev.* **138**, 3418–3433.

Winchell, M., Gupta, H. V. and Sorooshian, S. 1998. On the simulation of infiltration- and saturation-excess runoff using radar-based rainfall estimates: effects of algorithm uncertainty and pixel aggregation. *Water Resour. Res.* **34**, 2655–2670.

Wulfmeyer, V., Behrendt, A., Bauer, H.-S., Kottmeier, C., Corsmeier, U. and co-authors. 2008. The Convective and Orographically-induced Precipitation Study: a Research and Development Project of the World Weather Research Program for improving quantitative precipitation forecasting in low-mountain regions. *Bull. Am. Meteorol. Soc.* **89**, 1477–1486. DOI: 10.1175/2008BAMS2367.1.

Wulfmeyer, V., Behrendt, A., Kottmeier, C., Corsmeier, U., Barthlott, C. and co-authors. 2011. The Convective and Orographically Induced Precipitation Study (COPS): the Scientific Strategy, the Field Phase, and First Highlights. COPS Special Issue. *Q. J. Roy. Meteorol. Soc.* **137**, 3–30. DOI: 10.1002/qj.752.

Xiao, Q. and Sun, J. 2007. Multiple-radar data assimilation and short-range quantitative precipitation forecasting of a squall line observed during IHOP_2002. *Mon. Weather Rev.* **135**, 3381–3403.

Xue, M., Kong, F., Thomas, K. W., Gao, J., Wang, Y. and co-authors. 2013. Prediction of convective storms at convection-resolving 1 km resolution over continental United States with radar data assimilation: an example case of 26 May 2008 and precipitation forecasts from spring 2009. *Adv. Meteorol.* **2013**, 1–9.

Zupanski, D., Zhang, S. Q., Zupanski, M., Hou, A. Y. and Cheung, S. H. 2011. A prototype WRF-based ensemble data assimilation system for dynamically downscaling satellite precipitation observations. *J. Hydrometeorol.* **12**, 118–134.